Electronic Supplementary Material (ESI) for Physical Chemistry Chemical Physics.

Shortwave Infrared Polymethine Dyes for Bioimaging: Ultrafast Relaxation Dynamics and Excited-State Decay Pathways

*Laura M. Obloy, Steffen Jockusch, Alexander N. Tarnovsky**

Department of Chemistry and the Center for Photochemical Sciences, Bowling Green State University, Bowling Green, OH 43403, USA

AUTHOR INFORMATION
Corresponding Author
* E-mail: atarnov@bgsu.edu

Methodological details

Construction of stimulated emission cross-section spectra. The analysis of transient absorption spectra requires the knowledge of S_1-S_0 stimulated emission (σ_{SE}) cross-section spectra. To obtain the σ_{SE} spectrum, it is necessary to divide the fluorescence spectrum $I_f(\lambda)$ by a factor of ν^4, where ν is the frequency of the emitted light. The ν^4 factor arises because the energy bandwidth of the emission monochromator is proportional to ν^2, but $I_f(\lambda)$ is proportional to ν^3 whereas σ_{SE} is proportional to ν. Further, the fluorescence and absorption spectra belong to the same S_0-S_1 electronic transition, and are approximately mirror symmetrical, which indicates that absorptive and emissive states undergo only minor changes of the nuclear geometry with respect to one another.[1] Therefore, the S_0-S_1 and S_1-S_0 transition dipole moments should be the same, implying that the areas under the $I_f(\lambda)$ spectrum divided by ν^5 (that is $\sigma_{SE}\nu^{-1}$) and the absorption spectrum divided by ν (that is $\sigma_A\nu^{-1}$) should be the same,[2] where the σ_A spectrum is obtained from the known extinction coefficient $\varepsilon(\lambda)$ spectrum, see the main text. Consequently, the σ_{SE} spectrum should be renormalized so that the $\sigma_{SE}\nu^{-1}$ spectrum yields the same area as the $\sigma_A\nu^{-1}$ spectrum. To do so, the σ_A spectra of Chrom7 and Flav7 were truncated at 712 and 708 nm, and the long-wavelength $\sigma_A\nu^{-1}$ parts assigned entirely to the S_0-S_1 transition were integrated, which yielded the renormalization factor of 1.140 and 1.233, and subsequently, the maximum values of $\sigma_{SE}(\lambda) = 1.09{\cdot}10^{-15}$ cm^2 and $\sigma_{SE}(\lambda) = 1.14{\cdot}10^{-15}$ cm^2 for Chrom7 and Flav7, respectively.

Ultrafast Transient Absorption. The set-up described previously[3,4] is based on a regeneratively amplified Ti:sapphire laser system (Hurricane, Spectra-Physics). The system output (800-nm, 90 fs, 0.9 mJ pulse^{-1}, 1 kHz repetition rate) is 50:50 split. The first portion is sent to an optical parametric amplifier, OPA, (TOPAS-C Light Conversion Lt.) to produce 1042-, 990-, and 925-nm (second harmonic idler) and 500-nm (sum frequency signal) pulses. They were sent through a 500 Hz chopper, and a Berek compensator to set the polarization plane to the magic angle (54.7°) with respect to that of the probe light, before being focused onto the sample. A broadband white-light continuum (wlc) in the 340-935 nm range and a single-wavelength OPA output tunable from 800 to 1160 nm were used for probing. The remaining part of the amplified output was sent to a variable time-delay stage, attenuated, and focused onto a 4-mm thick CaF_2 window to produce the wlc, which was focused onto the sample using the fully reflective optics. For single-wavelength probing, the remaining part of the amplified output was rerouted to pump another TOPAS-C, which output was attenuated, sent through the same delay stage, and then steered into the same optical path towards the sample as that of wlc. The probe and excitation beams overlapped at a 6° angle at the sample position, being 60 and 200 μm in diameter. A fraction of the probe beam split off before the sample was used as a reference for the correction of shot-to-shot pulse intensity fluctuations. The probe beam (after the sample) and the reference beam (bypassed the sample) were dispersed by a spectrograph/monochromator (Acton SP 2358) and recorded using either a dual diode array (Hamamatsu S8380-512Q) for the wlc probe or a photodiode pair (Hamamatsu S1337-66BQ) for the OPA probe; the detectors were synchronized to the 1 kHz repetition rate. The difference between the decadic logarithms of a probe-to-reference intensity ratio at a certain probe wavelength and a certain delay stage position

acquired for two consecutive laser shots, where for one the excitation is chopped (off) and for another the excitation excites the sample (on) is the transient absorption signal at the given delay time and the probe wavelength: $\Delta A = -log_{10}\left(\frac{I_{pr}}{I_{ref}}\right)_{on} - (-log_{10}\left(\frac{I_{pr}}{I_{ref}}\right)_{off})$. This signal is averaged using 300 pairs of consecutive laser system shots before moving to the next delay time and is further averaged over 20 to 50 delay line scans to yield the Δ*A* data point.

All experiments were performed at 22 °C unless stated otherwise and utilized a 2-mm pathlength rotating cell with typical concentrations of 0.015 mM for Flav7 (1042 nm excitation) and Chrom7 (990 nm excitation), 0.015 mM (925 nm excitation) and 0.05 mM (500 nm excitation) for both dyes. At these concentrations the sample absorbance obeyed the Lambert-Beer law. UV-vis absorption spectra measured before and after the experiments showed no change. Excitation energy measured at the sample position was 55 nJ (500 nm), 80 nJ (925 nm), or in the 45-60 nJ range for 990- and 1042-nm excitation. Such excitation conditions ensured that ΔA signals from Flav7 and Chrom7 depend linearly on excitation energy with the linear fit passing through the origin, Fig. S32; therefore, single-photon excitation is responsible for the measured data. Kinetic traces at the same probe wavelength measured using either wlc or single-wavelength OPA light were identical. To produce the full Δ*A* spectra in the 340–1160 nm range, the 340–935 nm wlc probe data, which were acquired in three visible, red, and near-IR windows, were merged with the data from the single-wavelength OPA probing (800–1160 nm). When probing in the wlc red and near-IR windows, appropriate long-pass color filters were placed on the spectrograph slit to eliminate second-order diffraction. Additionally, when probing in the near-IR window a 1-mm cell with a dye solution (IR132 in CH_2Cl_2) was placed on the slit to attenuate the residual 800-nm fundamental.

The ΔA signals from neat CH_2Cl_2 were measured immediately after experiments on Flav7 and Chrom7 and under the same excitation conditions; they were about 20-100 times smaller around zero delay time than the corresponding solute Δ*A* signals and not present past the initial ~170 fs (Fig. S33a-c). The solvent Δ*A* signals were shaped as two negative dips flanking a positive hump, as expected for the cross-phase modulation signals due to electronic instantaneous response of the solvent.[5,6] The cross-correlation function (CCF) between the excitation pulse and spectral components of the wlc pulse can be obtained by considering how the slope of cross-phase modulation signals changes over time as described in the literature;[5] we found the CCF to be Gaussian-shaped with the full-width-at-half-maximum (fwhm) of 125 fs for 990- and 1042-nm excitation, and 145 fs for 925-nm excitation. The shape and width of the CCF function between 500-nm excitation and wlc probe pulses (Gaussian, 145-fs fwhm, Fig. S33d) was determined using the solvent anti-Stokes Δ*A* signal centered at time zero,[7] which is positioned at 433 nm and due to the Raman-active C-H stretching mode of CH_2Cl_2 (3045 cm^{-1} [8]). Using the solvent signals and DAFit software (Pascher Instruments AB, Lund, Sweden), Δ*A* data were corrected for group-velocity dispersion in the wlc probe light with a 20-fs accuracy. When probing in the near-IR with the OPA, Δ*A* signals from CH_2Cl_2 were even smaller, and therefore, the time zero and CCF were determined via sum-frequency (SF) mixing of the excitation and probe light in a 0.1-mm thick, type-I BBO crystal placed at the sample position. The temporal profile of the SF intensity is found to be bell-shaped with a 140-150 fs (990-nm excitation) and a 175 fs (1042-nm excitation) fwhm (Fig. S34). Time zero

determination was within ~20 fs. An instantaneous Δ*A* signal rise observed at 1140- and 1160-nm probe wavelengths following 1042-nm excitation of Flav7 yields a somewhat shorter CCF fwhm of 136 and 164 fs. Therefore, in the OPA probe experiments the CCF fwhm is considered to be ~155 fs.

Low-temperature S_1-state lifetime measurements were performed upon 1042-nm (Flav7) and 990-nm (Chrom7) excitation and the wlc probe. The samples (solvent: ACS-grade anhydrous $CHCl_3$, Fischer Scientific) were kept in a 1×1×4 cm^3 quartz cell immersed into a Dewar condenser filled with acetone cooled by liquid N_2, where the temperature was monitored with a thermocouple.

Multiexponential fits of representative Δ*A* kinetic traces with CCF deconvolution (as implemented in Spectra Solve 2.01 Pro software package, Lastek Pty. Ltd) were carried out, from which the time resolution in the experiments reported herein is 40 fs. The software program OriginPro version 7 (Origin Lab Corporation, Northampton, MA, USA) was used for exponential fitting of the data at delay times longer than 200 fs. In both methods, up to a sum of six exponential decay functions were used, represented by the expression $\Delta A = \sum_{i=6} A_i(\lambda) e^{-t/\tau_i}$, where $A_i(\lambda)$ is the amplitude and τ_i is the time constant of the i^{th} component. Fast Fourier Transform (FFT) analysis was performed on the residuals of multiexponential fits using the OriginPro software.

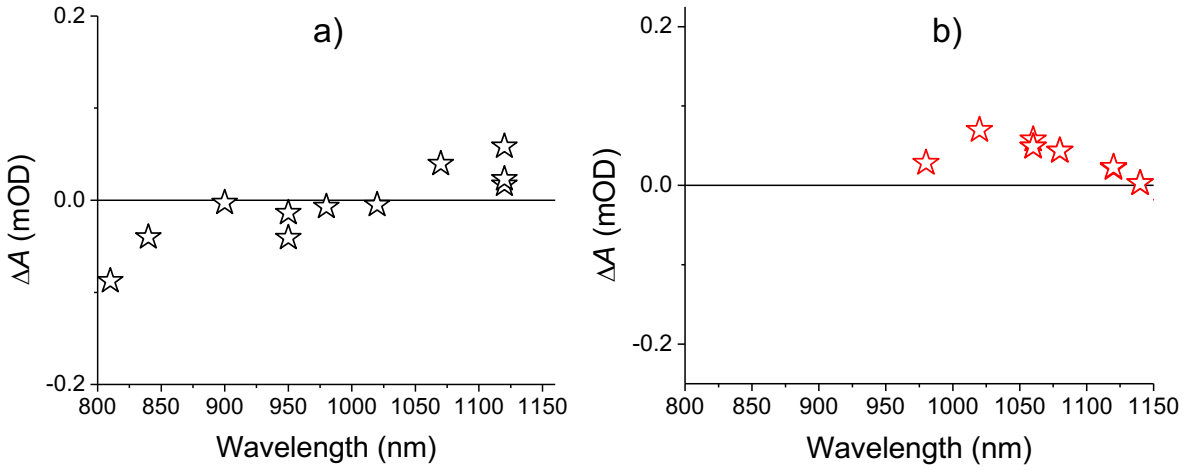

Fig. S1. Chrom7 excited at 990 nm, a), and Flav7 excited at 1042 nm, b): small ΔA signals persistent between 1 and 2 ns were time-averaged between these delay times and the resulting average is shown (symbols). The 1-2 ns long-time ΔA data points from the independent measurements of ΔA kinetic traces were reproducible. Measuring these residual signals more accurately is restricted by the signal-to-noise limitations. Even though a larger ΔA signal would be produced by increasing the excitation energy, an excitation energy more than what was used in these experiments (~50-70 nJ pulse^{-1}) would exceed the optical saturation energy and saturate the S_0-S_1 absorption transition, Fig. S32, which would cause secondary excitations within the same excitation pulse and make the data interpretation unreliable.

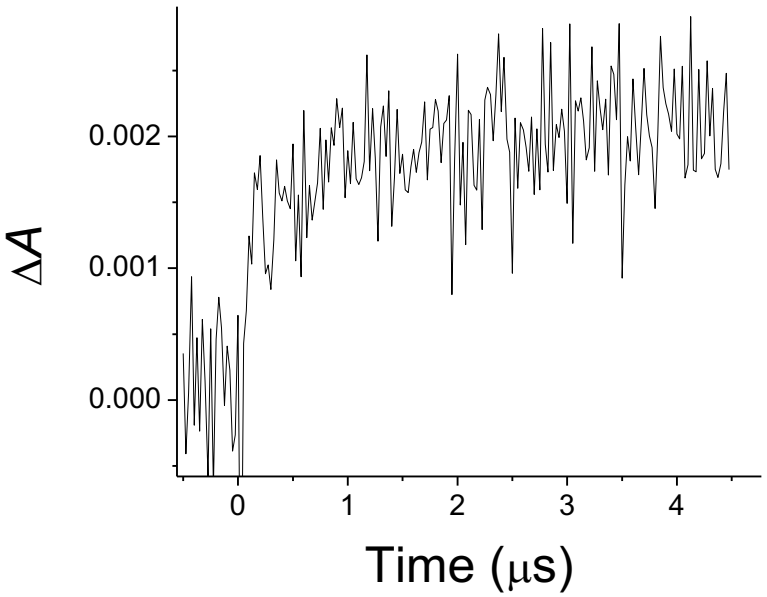

Fig. S2. The transient absorption scan shown is recorded after a nanosecond pulsed 532-nm excitation of Chrom7 in CH_2Cl_2. The induced absorption of Chrom7 in CH_2Cl_2 at a 600-nm probe wavelength is persistent when the solution is saturated with a O_2 quencher of excited triplet states[9]; the Chrom7 signal does not decay as expected if it were of the triplet-triplet absorption nature. In the experiment, the sample was saturated with O_2 by bubbling it through the solution.

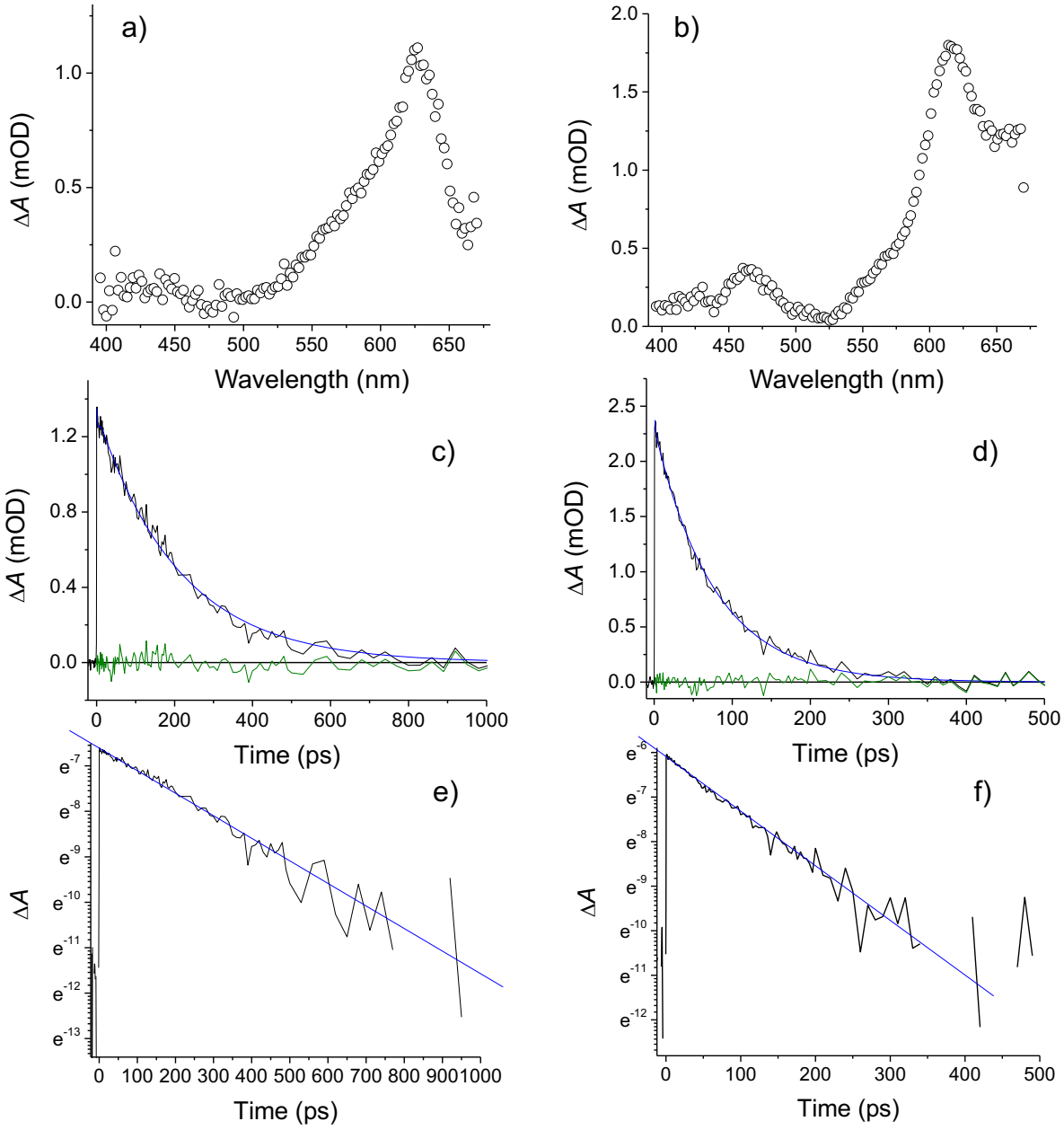

Fig. S3. Representative transient absorption data for $CHCl_3$ solution (22 °C) of Chrom7 in a), c), and e) following 990-nm excitation, and Flav7 in b), d), and f) following 1042-nm excitation. The ΔA spectra are shown at 50 ps in a), Chrom7, and 20 ps in b), Flav7, and illustrate ESA from the S_1 state. The ΔA kinetic traces at a probe wavelength of 630 nm in c), Chrom7, and 620 nm in d), Flav7, are dominated by the decay with a time constant of 210 $\pm$ 3 ps for Chrom7 and 77 $\pm$ 2 ps for Flav7 ascribed to the S_1-state lifetime τ_f, see also the natural logarithmic plots of the same data in e) and f). The fits (blue) and fit residuals (green) are shown in c) and d); we used a three-exponential decay fitting model, where the first two components (sub-1 ps and a few ps) were minor in amplitude, and therefore, not reported.

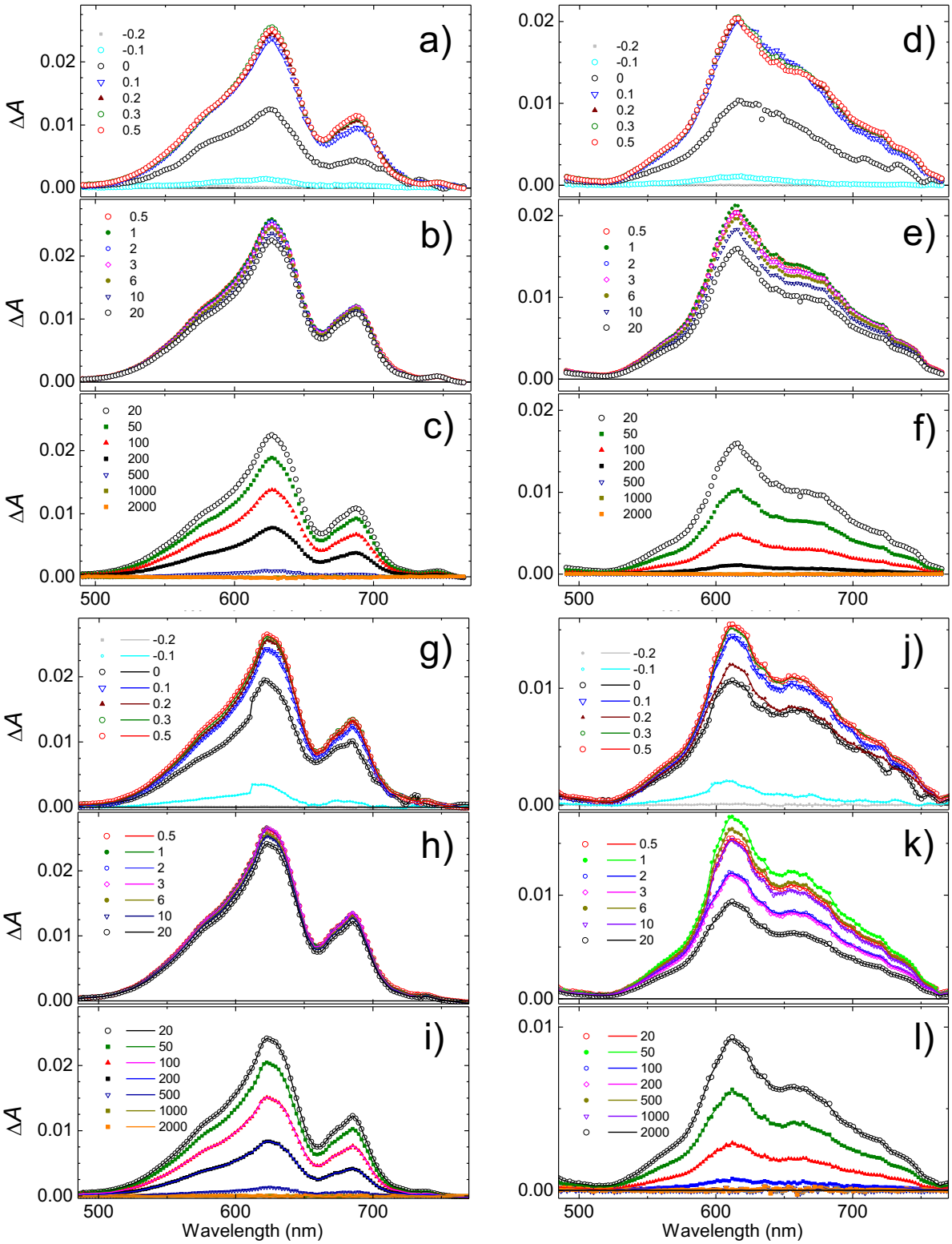

Fig. S4. Comparison of ΔA spectra of Chrom7 (a-c and g-i) and Flav7 (d-f and j-l) in CH_2Cl_2 at short (a, d, g, j), intermediate (b, e, h, k), and long (c, f, i, l) times after excitation. Delay times between the excitation and probe pulses are given in the legends. Excitation is at 925 nm, a-c) for Chrom7 and d-f) for Flav7, 990 nm for Chrom7, g-i), and 1042 nm for Flav7, j-l).

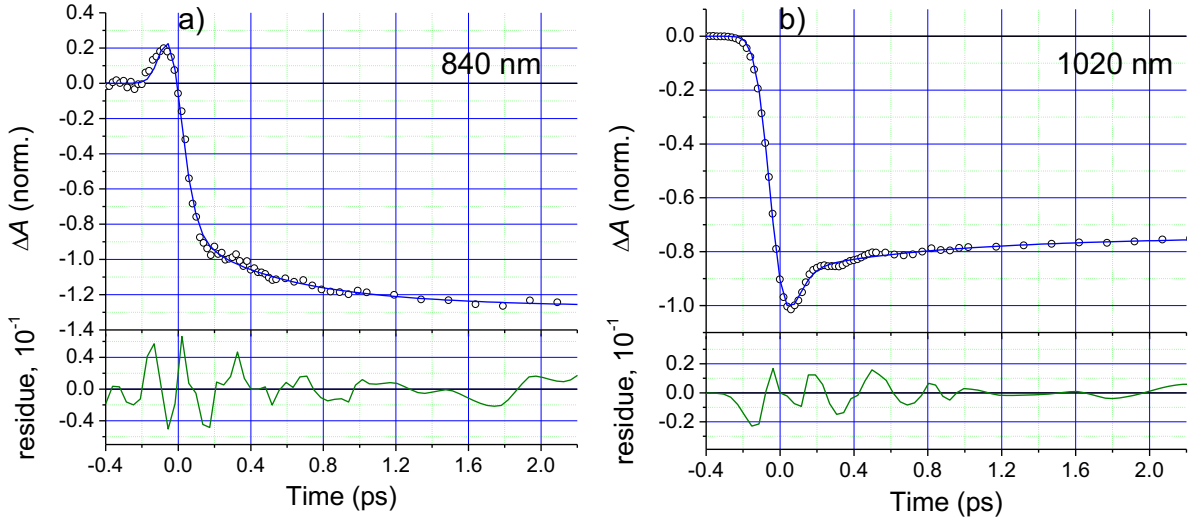

Fig. S5. Chrom7 excited at 990 nm. Normalized short-time 840- and 1020-nm ΔA kinetic traces, a) and b). A ~1 ps time component is evidently present. Multiexponential fits (blue) of the data and fit residuals (green) are also shown. The fits were performed with CCF deconvolution, where the CCF fwhm is 125 fs at 840 nm and 150 fs at 1020 nm. The best fit time constants and amplitudes (given in parentheses) are as follows: 46 fs rise (–144%), 380 fs rise (–22%), 1.0 ps rise (–18%), 165 ps decay (100%) at 840 nm, and 28 fs rise (–59%), 40 fs decay (72%), 350 fs decay (0.7%), 0.83 ps decay (3.5%), 165 ps decay (24%) at 1020 nm. Here and thereafter, all fit amplitudes at a given probe wavelength are reported with respect to a sum of the decay (i.e., positive) amplitudes taken to be 100%.

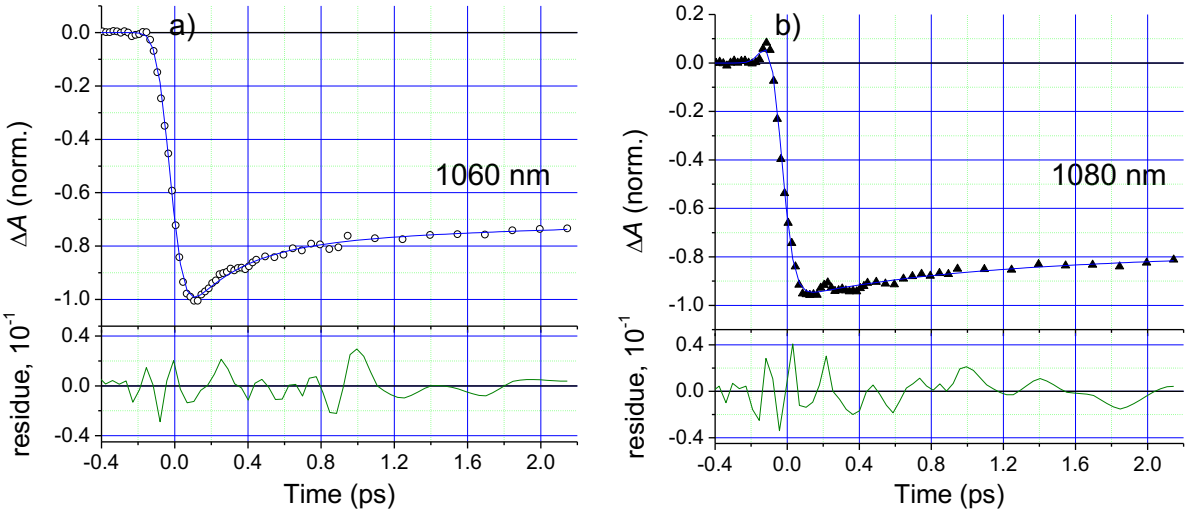

Fig. S6. Flav7 excited at 1042 nm. Normalized short-time 1060- and 1080-nm ΔA kinetic traces, a) and b). A ~1 ps decay component is evidently present. Multiexponential fits (blue) performed with CCF deconvolution (CCF fwhm, 125 fs) and fit residuals (green) are also shown. The best fit time constants and amplitudes (given in parentheses) are as follows: 25 fs rise (–50%), 204 fs decay (27%), 1.0 ps decay (10%), 65 ps decay (63%) at 1060 nm, and 28 fs rise (–140%), 0.87 ps decay (14%), 65 ps decay (86%) at 1080 nm.

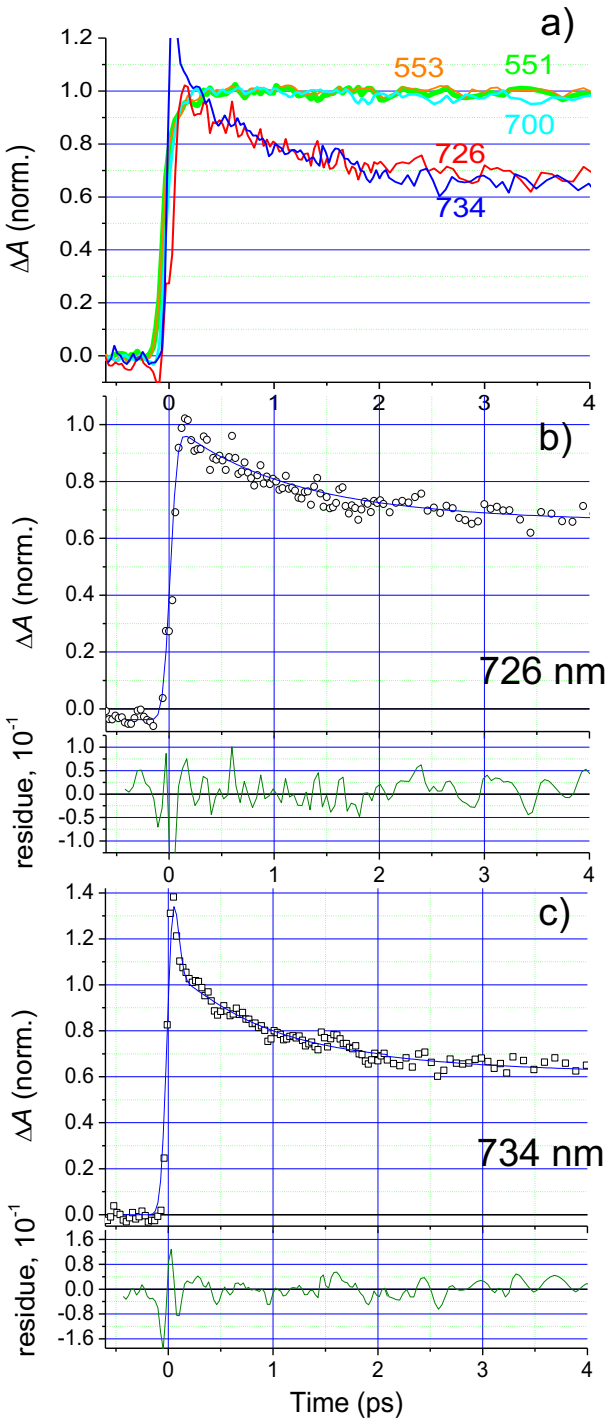

Fig. S7. Chrom7, λ_{exc} = 990 nm. Normalized short-time ΔA kinetic traces at several representative probe wavelengths, a). The ~1 ps time component evidently occurs in the red probing region, where there is the appreciable S_0-S_1 absorption; the amplitude of this component grows at longer probe wavelengths. Multiexponential fits with CCF deconvolution (CCF fwhm, 125 fs,) of the ΔA kinetic traces, b) and c), yield: 1.1 ps (31%) and 165 ps (69%) decay at 726 nm, and 157 fs rise (-3.9%), 0.9 ps decay (39.3%), 165 ps decay (61.7%), and a fast unresolved (<20 fs) component at 734 nm.

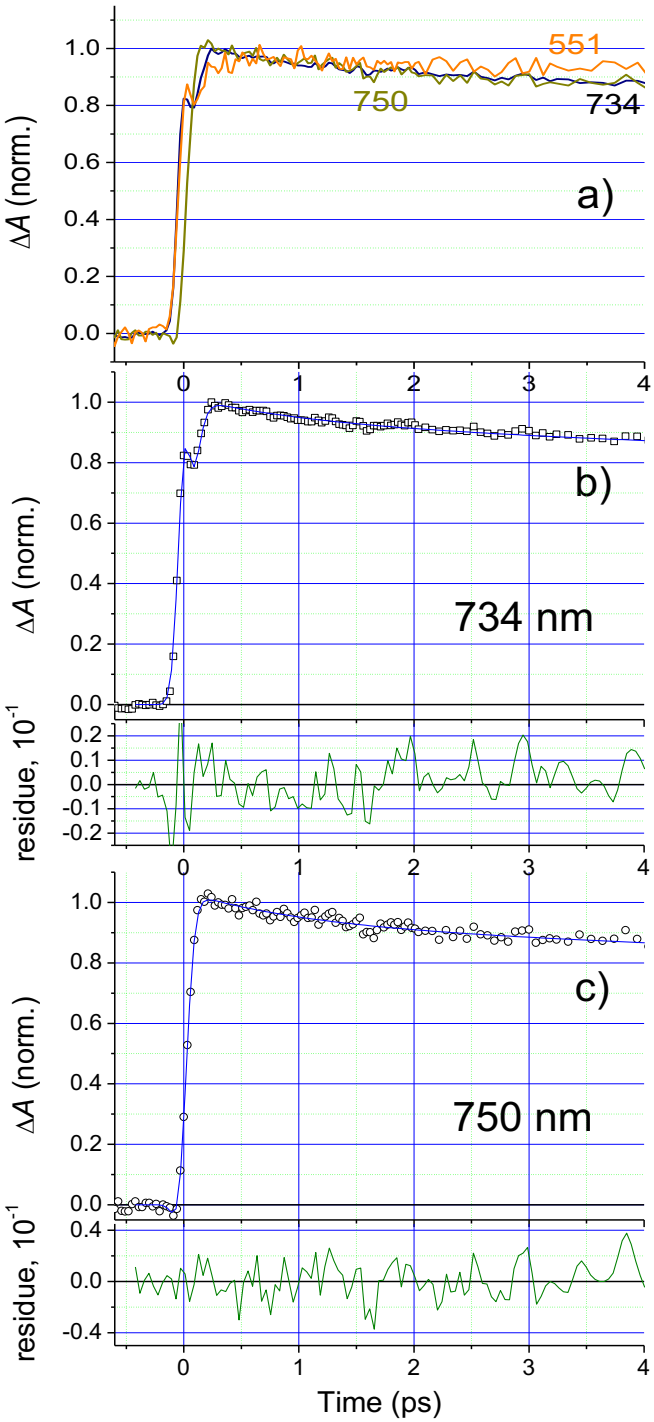

Fig. S8. Flav7, λ_{exc} = 1042 nm. Normalized short-time 551-, 734- and 750-nm ΔA kinetic traces. The ~1 ps time component predominantly occurs in the red probing region, where there is a significant S_0-S_1 absorption; the amplitude of this component increases as the probe wavelength becomes longer. Multiexponential fits with CCF deconvolution (CCF fwhm, 125 fs) yield: 20 fs decay (83%), 39 fs rise (–64%), 1.1 ps decay (2%), and 65 ps decay (15%) at 734 nm, b), and 30 fs rise (–147%), 1.1 ps decay (12%), and 65 ps decay (88%) at 750 nm, c).

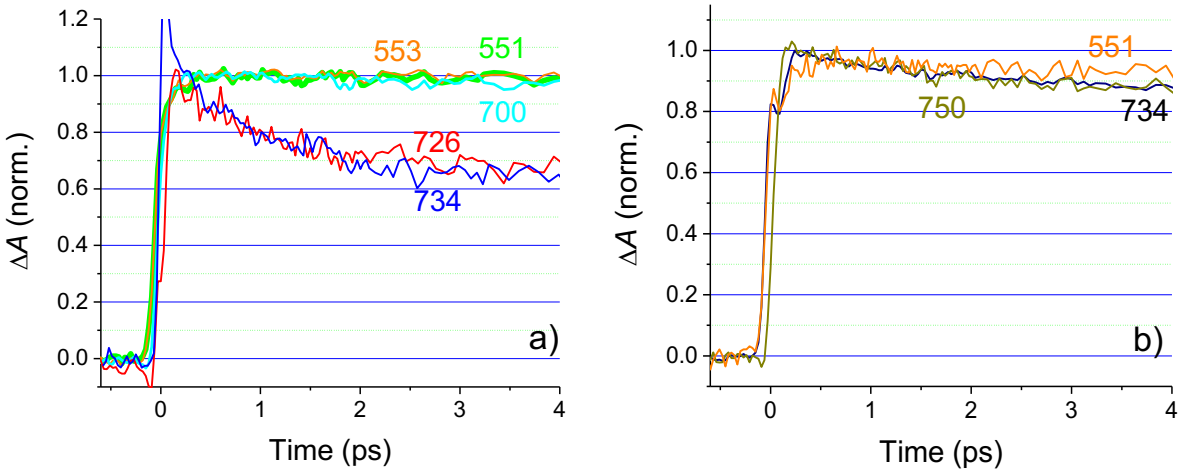

Fig. S9. Normalized representative ΔA kinetic traces shown in Fig. S7-S8 are compared; for Chrom7 for λ_{exc} = 990 nm, a), and Flav7 for λ_{exc} = 1042 nm, b). Because for Flav7, b), the S_0-S_1 absorption spectrum is significantly red-shifted with respect to the 720-750-nm probing region, the 1-ps time evolution at these probe wavelengths is less pronounced compared with Chrom7 in a).

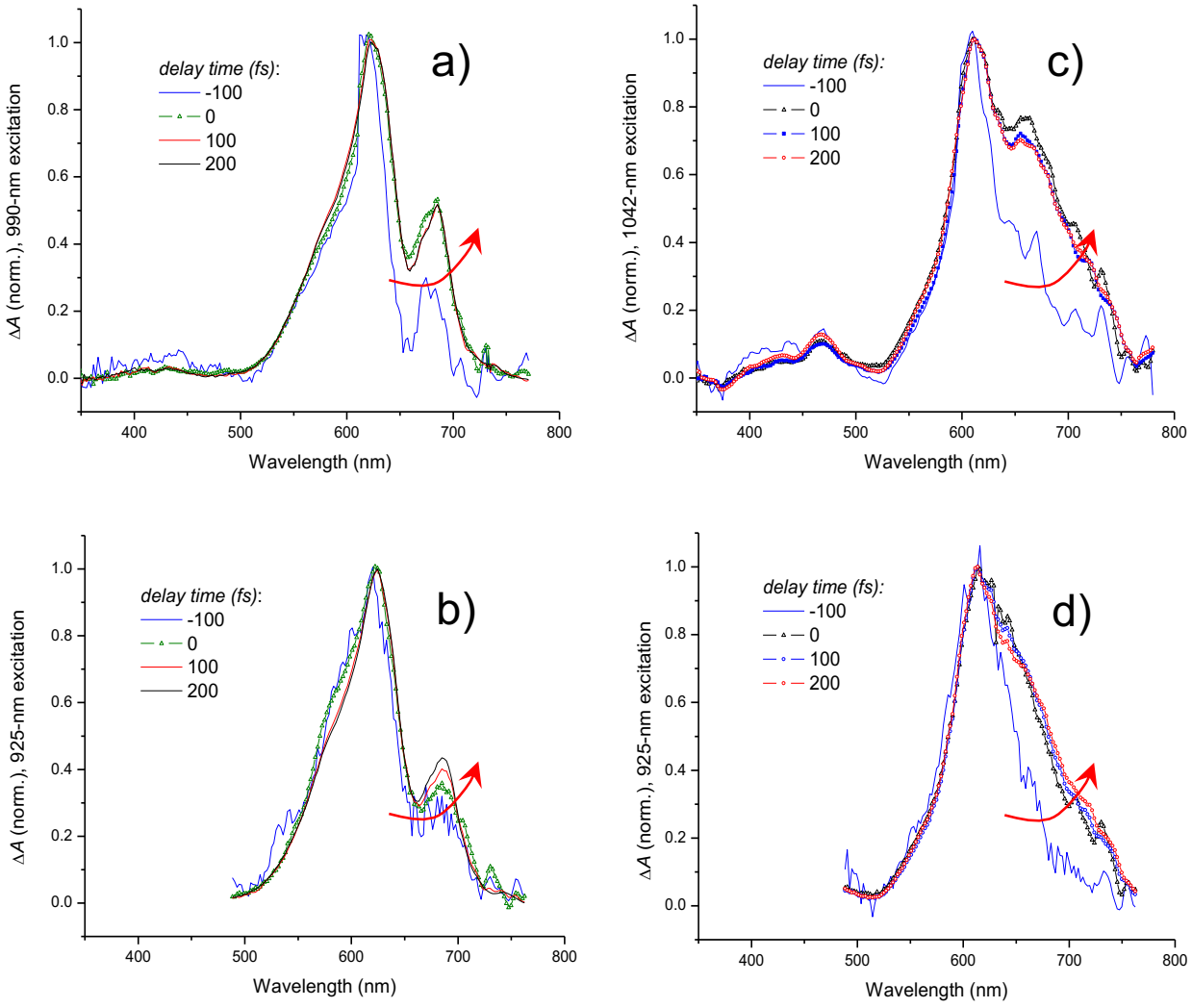

Fig. S10. Normalized Δ*A* spectra in the region of ESA from the S_1 state for Chrom7 corresponding to excitation at 990 nm in a), and 925 nm in b), and for Flav7 corresponding to excitation at 1042 nm in c) and 925 nm in d). The Δ*A* spectra illustrate hole shifting and broadening effects of the ground-state absorption hole, as indicated by the red arrows. This effect is major between delay times of –100 and 0 fs. For excitation at the low-energy side of absorption spectrum, a) and c), the hole replica in the S_1 state is stationary.

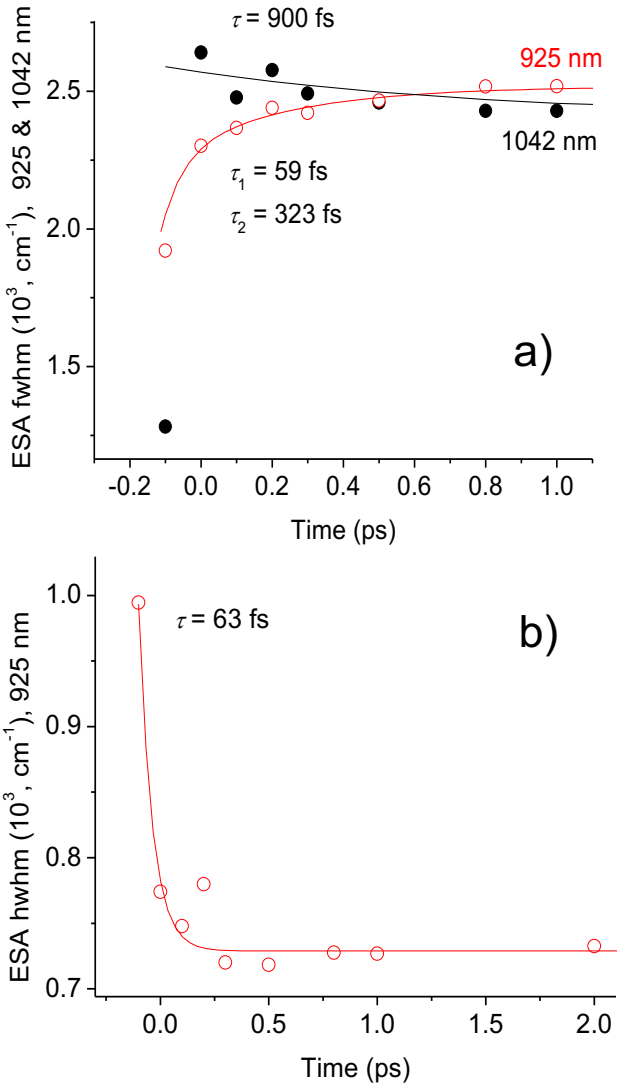

Fig. S11. Time evolution of the ESA width for Flav7. In a), narrowing of the ESA fwhm (1042 nm excitation) is modelled by a single-exponential decay with a 900-fs time constant. This narrowing is attributed to S_0 hole filling, thereby reducing the positive ΔA signal on the red side of the ESA region, Fig. S8a. More specifically, there exists a significant overlap with the linear S_0-S_1 absorption in this region; as the ground-state hole is slowly filled in, the entire linear absorption spectrum bleaches, but especially so in the red. Consequently, the amplitude of the 1 ps component increases as probe wavelengths are tuned to the red. There also exists a fast, 350-fs component of ground-state hole dynamics (Fig. 5, main text). Excitation at 925 nm prepares S_1 molecules with the excess vibrational energy. Since vibrational relaxation is mostly evident on the low-energy side of the ESA spectrum (Fig. S17), the fwhm evolution is affected by both hole-burning and vibrational relaxation dynamics. On the other hand, the hwhm evolution on the high-energy side of the ESA spectrum is less sensitive to vibrational relaxation. The fwhm, a), decays double-exponentially (time constants, 59 and 323 fs), whereas the hwhm, b), decays single-exponentially (time constant, 63 fs). The 59- and 63-fs time constants agree, and consequently, the 323-fs time constant is attributed to vibrational relaxation in the S_1 state following 925-nm excitation.

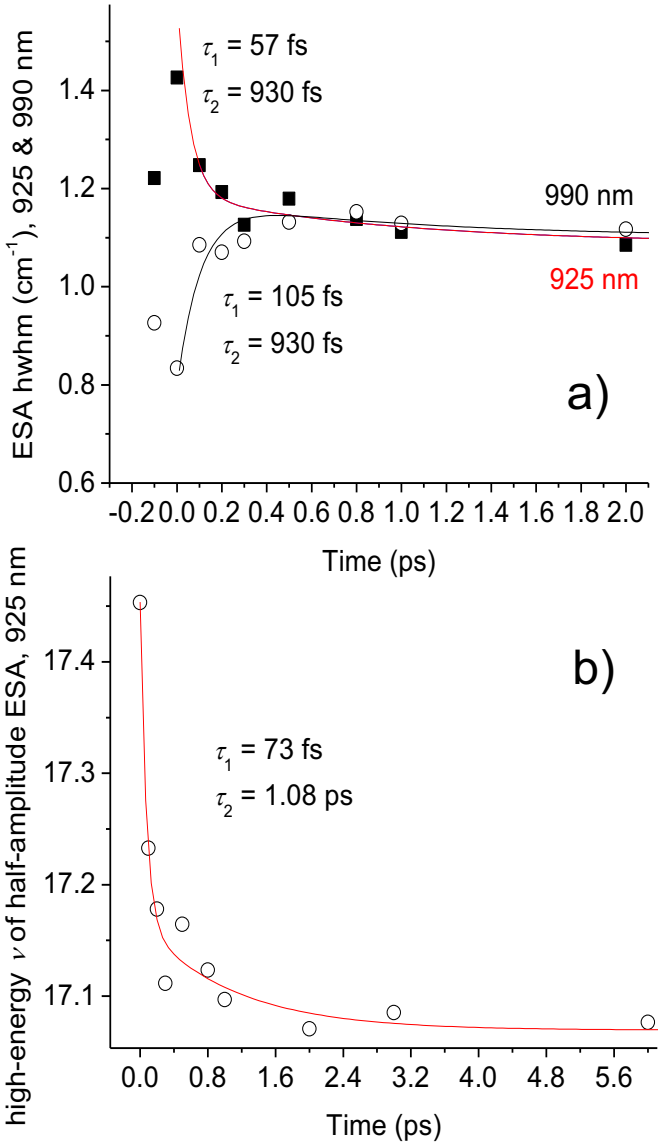

Fig. S12. The ESA width for Chrom7 as a function of time. Vibrational relaxation in the S_1 state after 990- and 925-nm excitation is manifested through the relative amplitude and shape of the red, ~685-nm shoulder with respect to the main 625-nm ESA peak, main text. For that reason, the time evolution of the hwhm values at the high-energy side of the ESA spectrum is analyzed in a). For both 990- and 925-nm excitation, the hwhm time dependence decays with a 930-fs time constant, which is the same as the 1-ps component pronounced in the red probing region (Fig. S9a and Fig. S14) due to slow ground-state hole filling, similar to what is discussed for Flav7 in Fig. S11. The initial hwhm evolution is attributed to a fast component of ground-state hole dynamics. The high-energy region of ESA is weakly sensitive to vibrational relaxation (all ΔA spectra in Fig. S17c, apart from that at 0 fs delay time, closely overlap in this region). Also, the S_0-S_1 absorption is not significant at the high-energy frequency corresponding to a half-amplitude of the ESA 625-nm maximum. Consequently, the relative weight of the 1-ps component is minor in the time evolution of this frequency, b), and the evolution of the high-energy frequency is thus more representative of hole-burning dynamics.

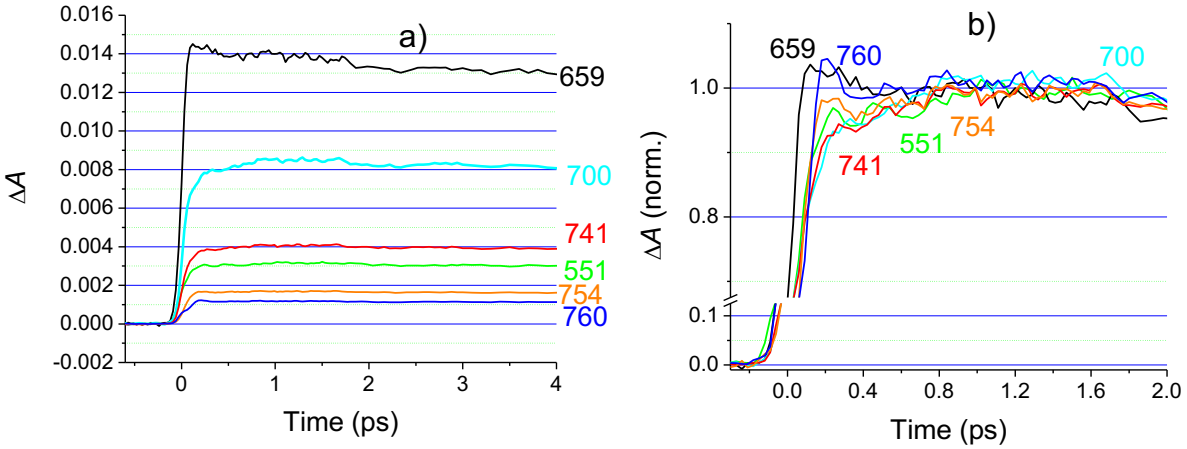

Fig. S13. Flav7, 925-nm excitation. Probe wavelengths are shown besides the ΔA kinetic traces. In b), the same ΔA data are shown, but normalized. It is evident from the arched shape of the ΔA kinetic traces that a ~1 ps time component is present, like the case of 1042-nm excitation of Flav7 (Fig. S9b).

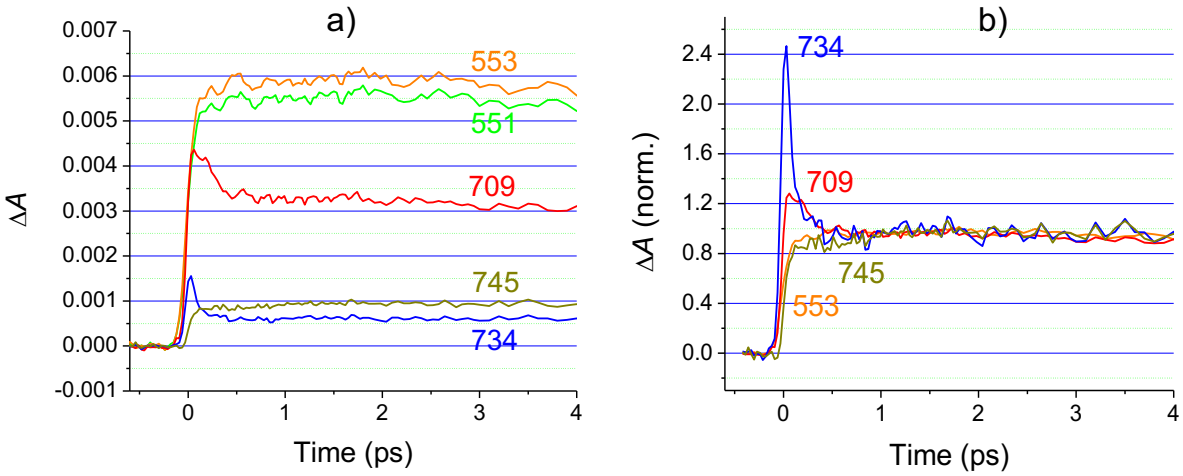

Fig. S14. Chrom7, 925-nm excitation. Short-time ΔA kinetic traces with the probe wavelengths given besides the kinetic traces. In b), the same ΔA data are shown, but normalized. It is evident from the slightly arched shape of the ΔA kinetic traces that a ~1 ps time component is present upon 925-nm excitation, similar to the case of 990-nm excitation of Chrom7 (Fig. S9a) as well as 1042- and 925-nm excitation of Flav7 (Fig. S9b and Fig. S13).

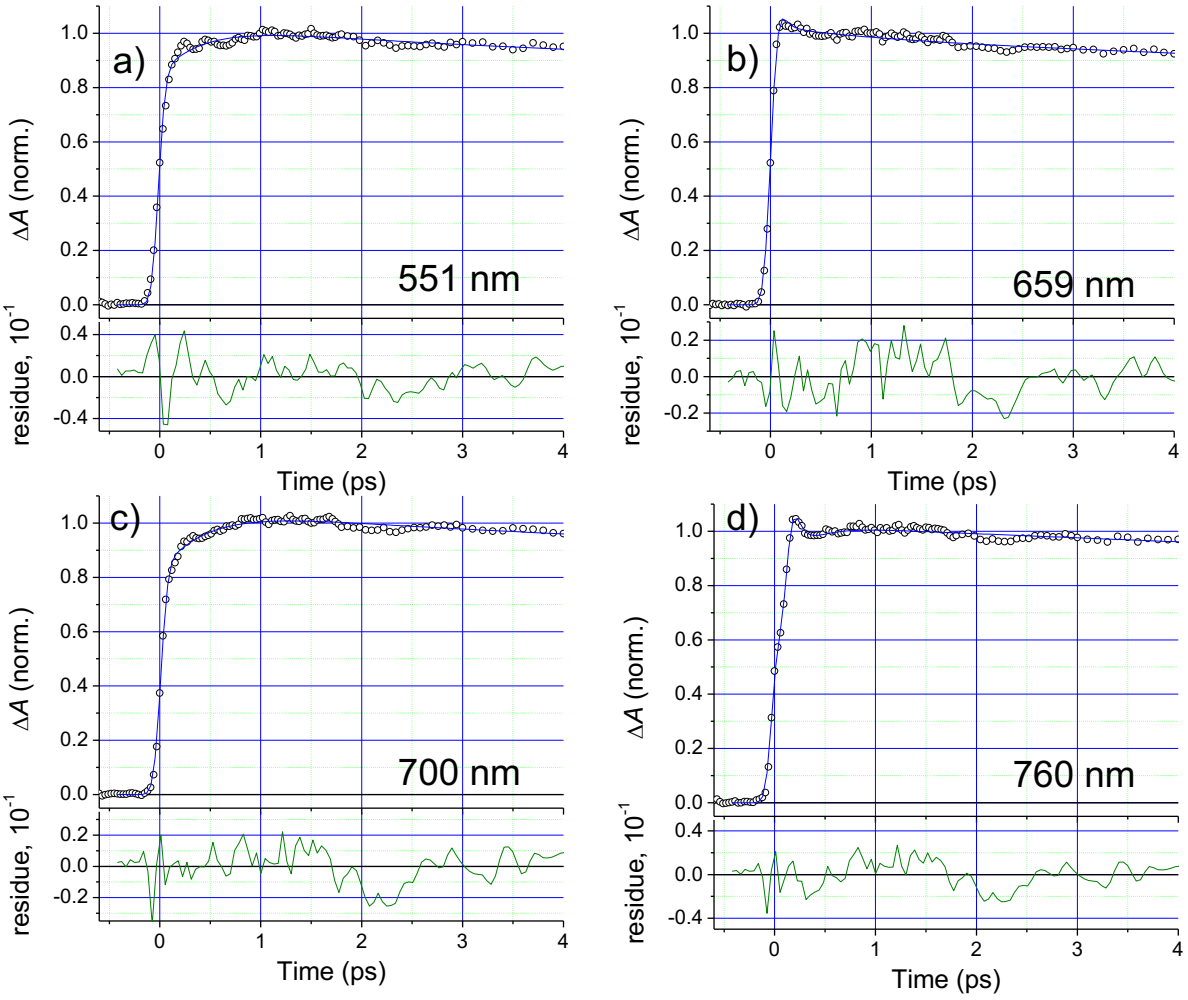

Fig. S15. Flav7, 925-nm excitation. Multiexponential fits with CCF deconvolution (CCF fwhm,125 fs) are shown for the ΔA kinetic traces given in Fig. S13. The fit residuals are shown in the panels below. The fits suggest that in addition to the 1-ps time constant present, there is a faster dynamics (time constants: 440 fs rise at 551 nm and 350 fs rise at 700 nm), which is in line with the ΔA spectral width dynamics, and can be, therefore, assigned to vibrational relaxation in S_1. Even faster components present (decay time constants: 60 fs at 659 nm and 43 fs at 760 nm) can be attributed to hole dynamics.

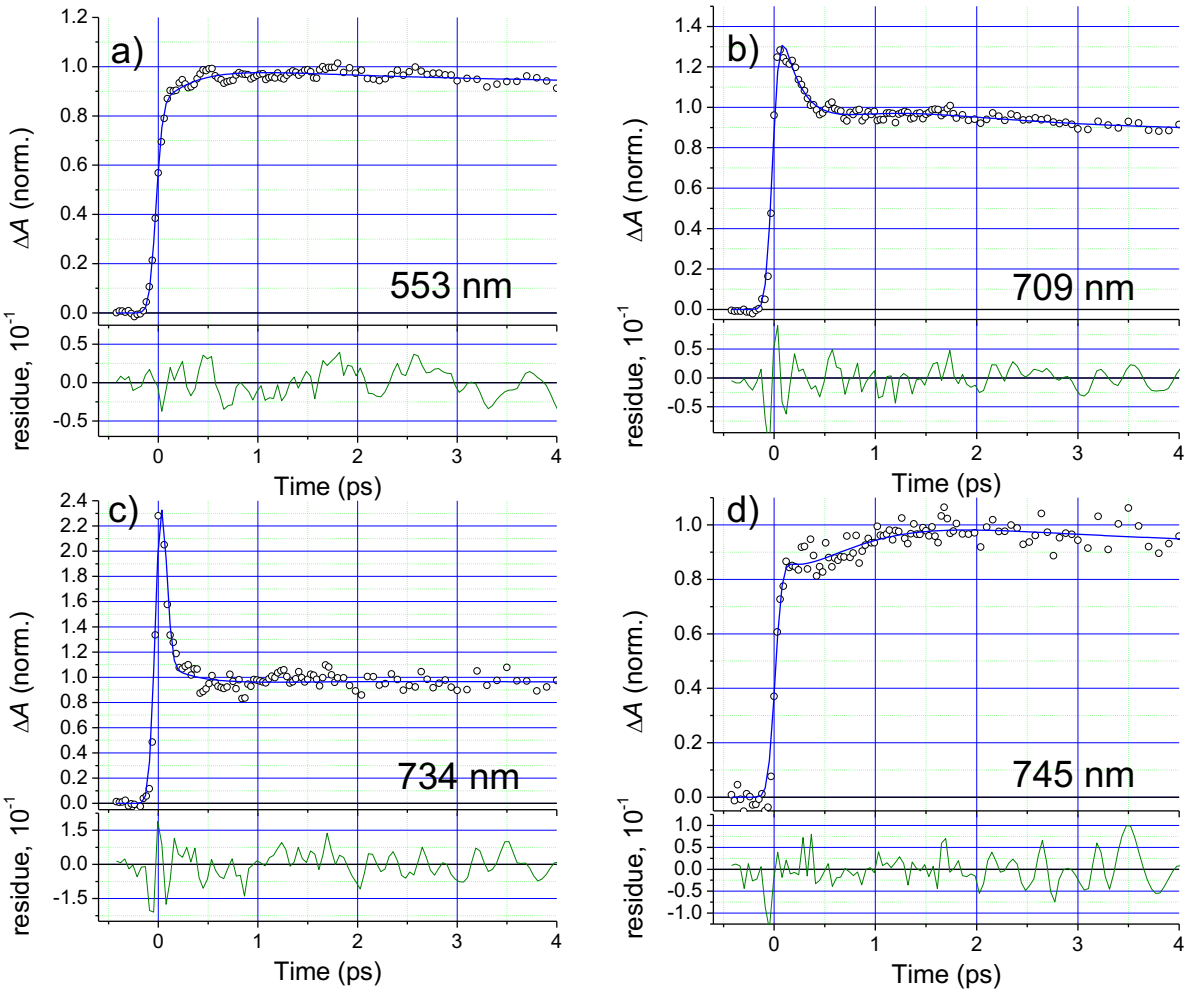

Fig. S16. Chrom7, 925-nm excitation: multiexponential fits with CCF deconvolution (CCF fwhm, 125 fs) of the ΔA kinetic traces shown in Fig. S14. Probe wavelengths are shown besides the kinetic traces with fit residuals given in the panels below. The fits suggest that in addition to the 1-ps time constant present, there is a faster dynamics assigned to vibrational relaxation in S_1 (time constants: 390 fs at 553 nm and 323 fs at 734 nm, and 445 fs at 745 nm), see also Fig. S15. Sub-100 fs time constants (83 fs at 709 nm and 445 fs at 745 nm) can be assigned to hole dynamics.

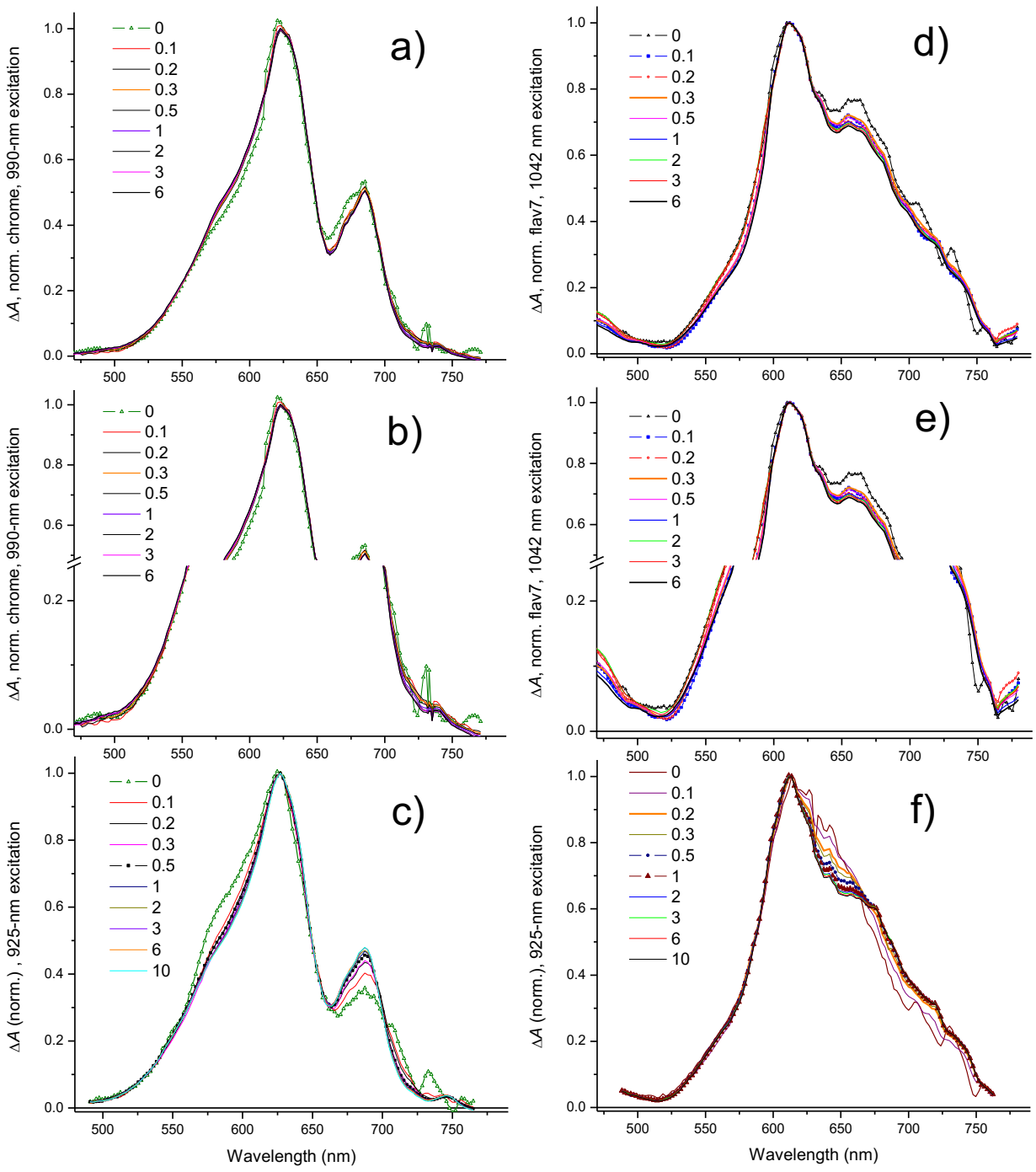

Fig. S17. Normalized Δ*A* spectra measured in the ESA region for Chrom7, 990-nm excitation in a) and b), note the vertical scale break, and 925-nm excitation in c), and for Flav7, 1042-nm excitation in d) and e), note the vertical scale break, and 925-nm excitation in f). Delay times between excitation and probe pulses are expressed in picoseconds and given in the legends. The Δ*A* spectra illustrate spectral broadening/narrowing effects. These are pronounced for the case of 925-nm excitation, c) and f), on the red side of the ESA spectrum from 0.1 to 0.5 ps (or, to ~1.0 ps) and attributed to mainly vibrational relaxation as this excitation wavelength accesses the 0-1' vibronic band of the S_0-S_1 transition.

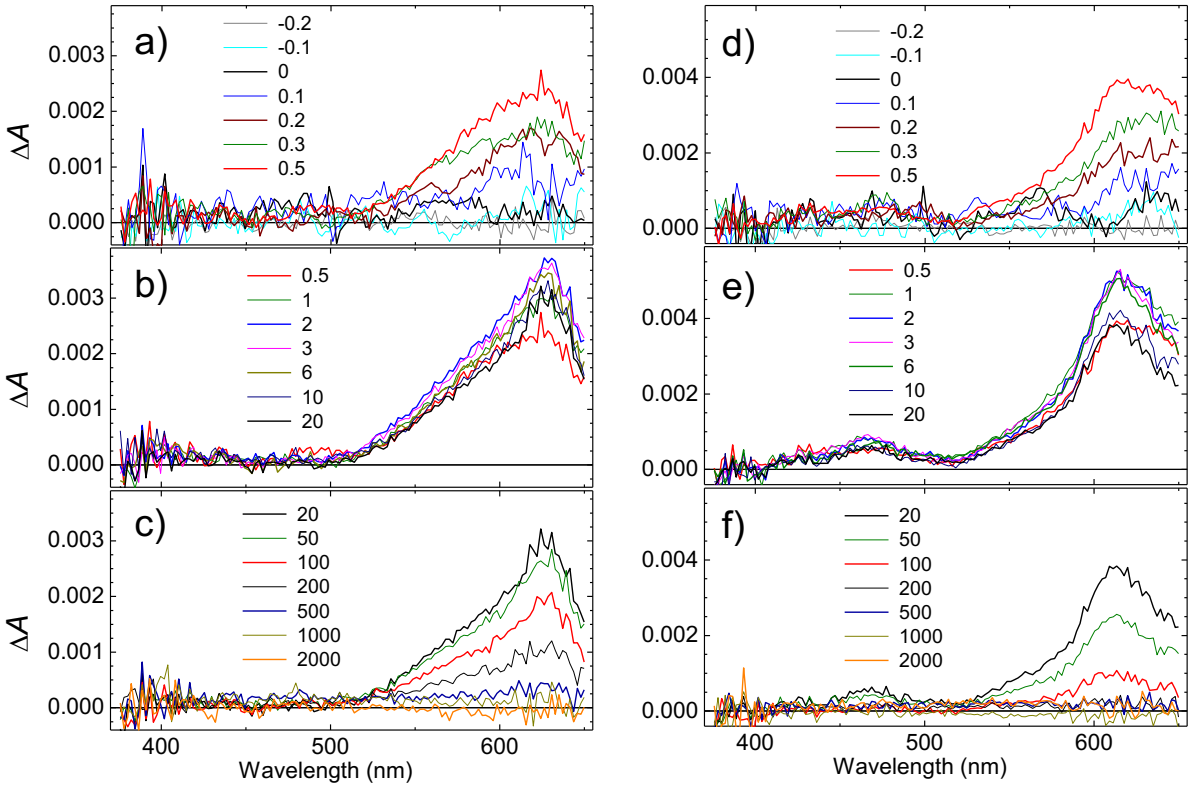

Fig. S18. The Δ*A* spectra measured following 500-nm S_0-S_n excitation of Chrom7, a-c) and Flav7, d-e). Short-time, a) and d), intermediate-time, b) and e), and long-time, c) and f) Δ*A* spectra are shown. Delay times between excitation and probe pulses (expressed in picoseconds) are given inside each panel.

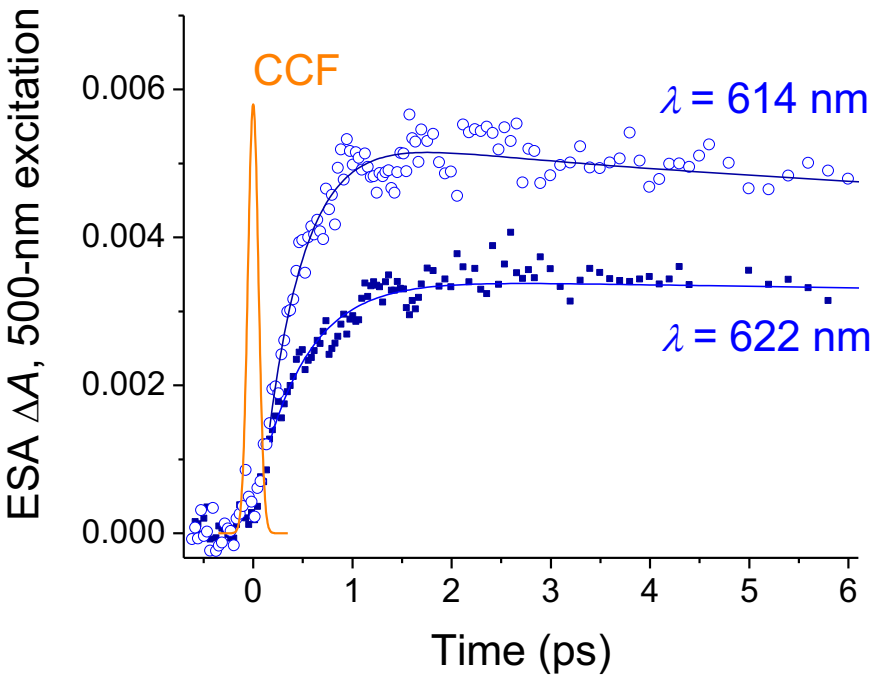

Fig. S19. The Δ*A* kinetic traces (symbols) at representative 614-nm (Flav7) and 622-nm (Chrom7) probe wavelengths measured for these dyes following their 500-nm excitation. The CCF between 500-nm excitation and wlc probe pulses has a Gaussian shape with a 145 fs fwhm, as shown. The shape and width of the CCF function were determined using the Δ*A* signal measured in neat solvent due to strong anti-Stokes absorption[7] centered at zero delay, which in this case is due to the Raman-active C-H stretching mode of CH_2Cl_2 (3045 cm^{-1} [8]). The signal was positioned at 433 nm. Apart from this signal, and a strong negative Δ*A* signal around time zero at 590 nm due to stimulated Raman emission from the same mode on the Stokes side of the 500-nm pump, the solvent contribution to the measured Δ*A* data was negligibly small. Triexponential fits (lines) of these data are those taken from Fig. S21.

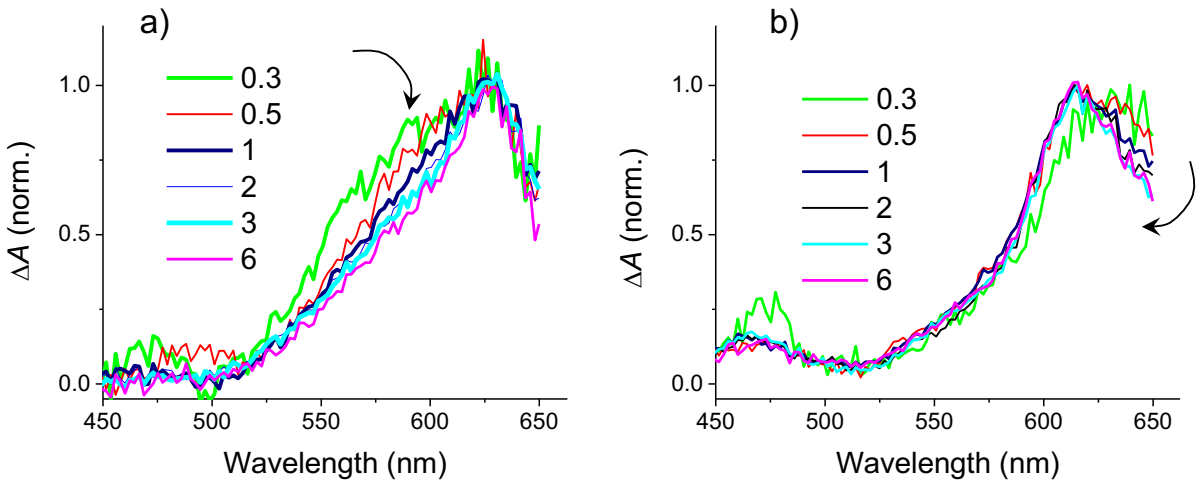

Fig. S20. Spectral narrowing of absorption from the excited S_1 state for Chrom7 in a), and Flav7 in b), following 500-nm excitation of these dyes. The arrows indicate the location and direction of the most prominent change. The corresponding spectral evolution take place between 0.3 and 3 ps. The multiexponential fits of the Δ*A* kinetic traces characterize this evolution by a 0.8 ps time constant, see Fig. S21.

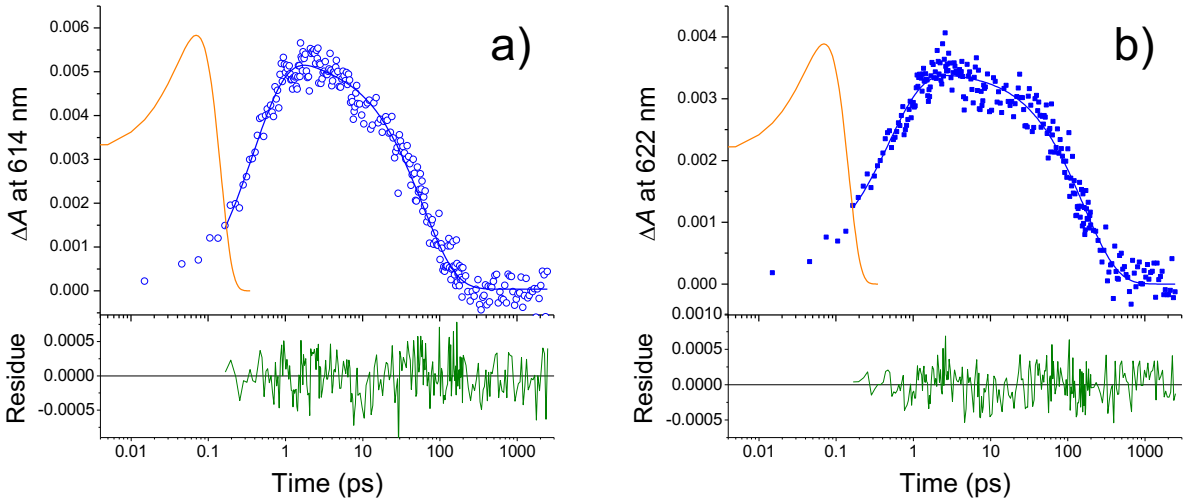

Fig. S21. The Δ*A* kinetic traces (symbols) measured at representative 614- and 622-nm probe wavelengths within the region of excited-state absorption from the S_1 state for Flav7 and Chrom7, respectively, following their 500-nm excitation. Note the logarithmic delay time scale. The shown Gaussian function at time zero illustrates the CCF between excitation and probe pulses (fwhm, 145 fs). The multiexponential fits (lines, carried out for delay times ≥110 fs) suggest the presence of three processes well-separated in time, which can be characterized by time constants of 0.4 ps (rise), 0.8 ps, and 160 ps (decay) for Chrom7 and 0.45 ps (rise), 0.8 ps, and 60 ps (decay) for Flav7. The 160 and 60 ps time constants are the S_1 lifetimes for Chrom7 and Flav7. These time constants were determined by fitting the data measured at single probe wavelengths within the ESA spectrum as well as by fitting the band integral $\int_{\bar{\nu}} \frac{\Delta A(\bar{\nu}) d\bar{\nu}}{\bar{\nu}}$ calculated over the ESA region, where $\bar{\nu}$ is the probe frequency expressed in the wavenumber units. Under the assumption that the oscillator strength of the ESA remains constant with time, which is a reasonable assumption on a tens of picosecond timescale when the equilibration processes are already complete, the value of the above integral is linearly proportional to the excited S_1-state population.[10] The 0.4 and 0.45 ps time constants are assigned to the population build-up in the S_1 state following decay from the initially excited 500-nm S_n state. The 0.8 ps time constant manifests itself as a rise or decay, depending on a probe wavelength, as expected for spectral broadening and narrowing, Fig. S19, and consequently, is assigned to vibrational relaxation in the S_1 state. Bottom panels show the residuals of 614- and 622-nm fits.

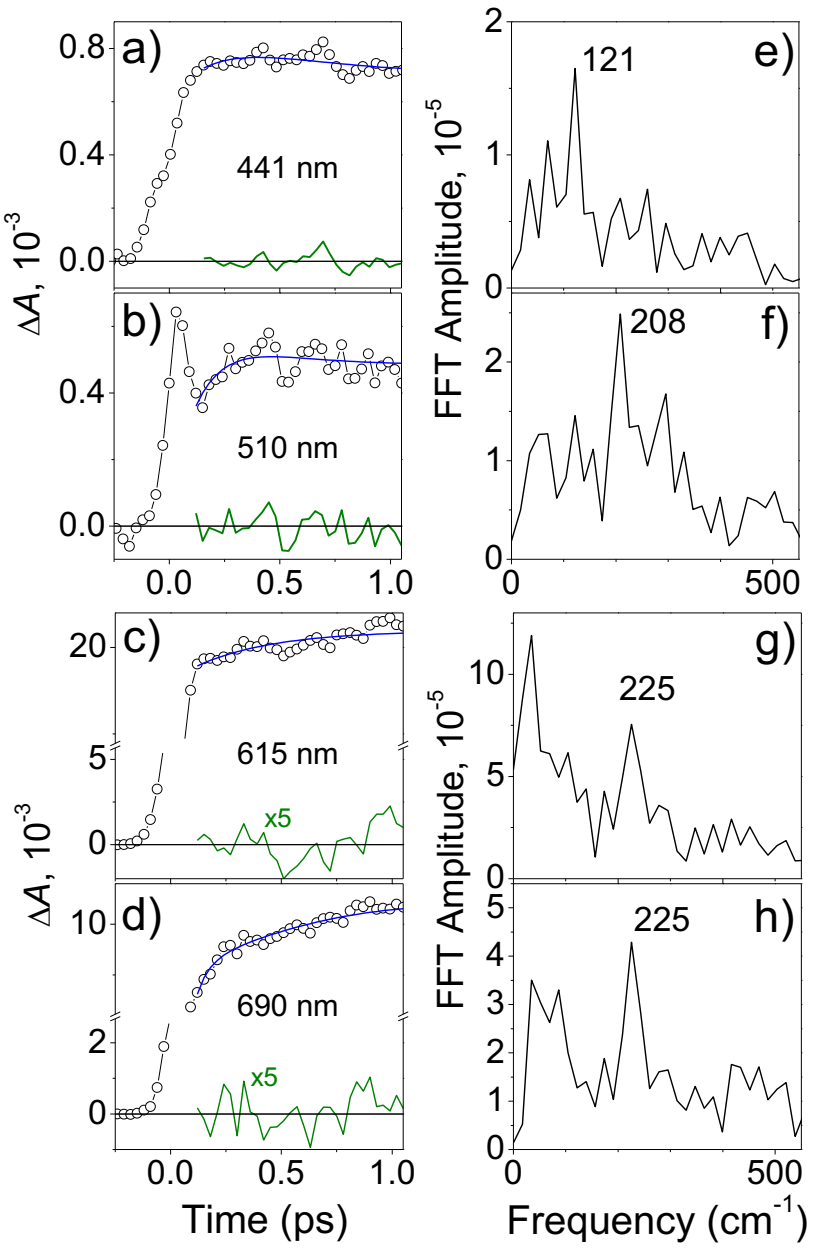

Fig. S22. In a-d), the short-time ΔA kinetic traces of Flav7 (symbols), multiexponential fits (blue), and fit residuals (green) at several representative probe wavelengths (indicated in each panel) following 1042-nm excitation, panels a) and b), and 925-nm excitation, panels c) and d). FFT analysis of the fit residuals in a-d) is shown in e-h), with the panels corresponding to each other row-wise.

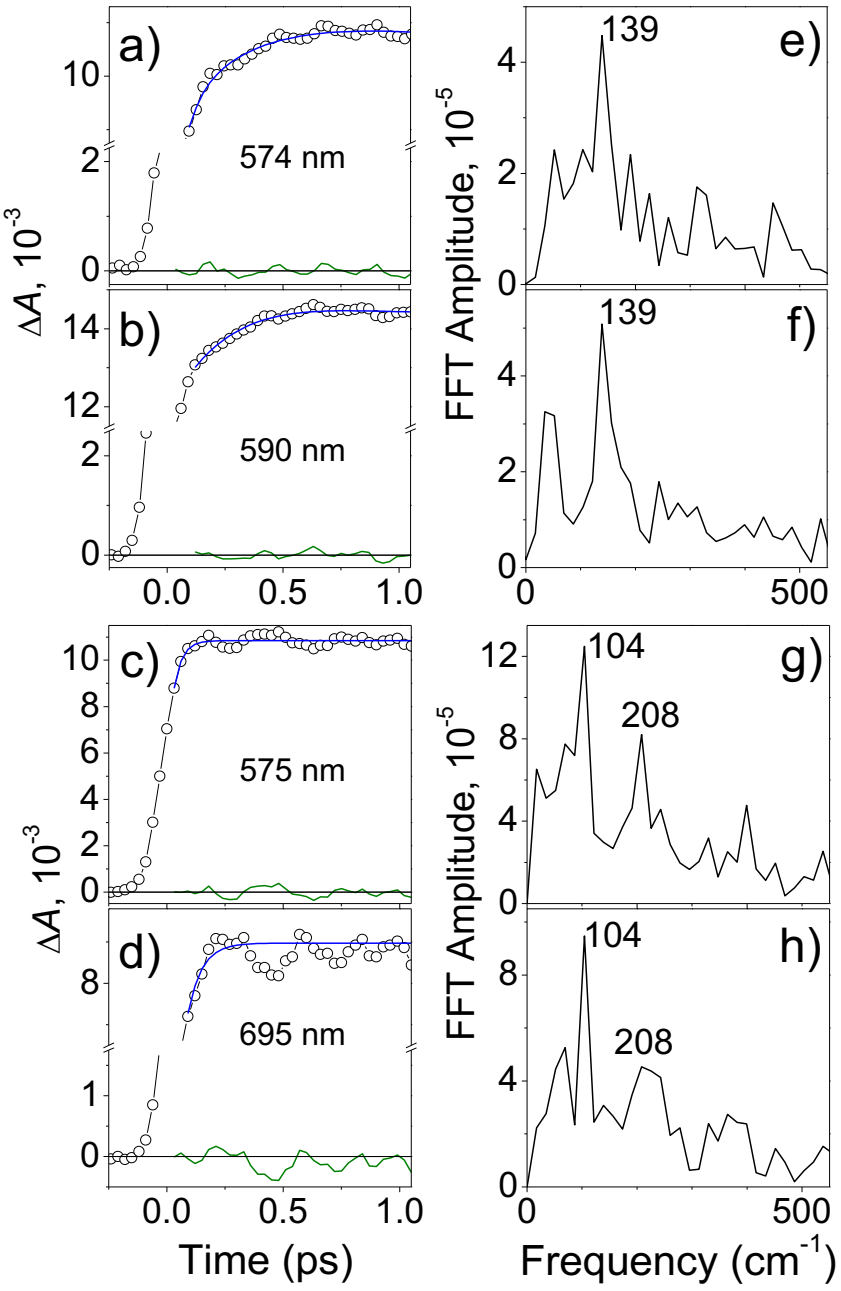

Fig. S23. In a-d), the short-time ΔA kinetic traces of Chrom7 (symbols), multiexponential fits (blue), and fit residuals (green) at several representative probe wavelengths (indicated in each panel) following 990-nm excitation, panels a) and b), and 925-nm excitation, panels c) and d). FFT analysis of the fit residuals in a-d) is shown in e-h), with the panels corresponding to each other row-wise.

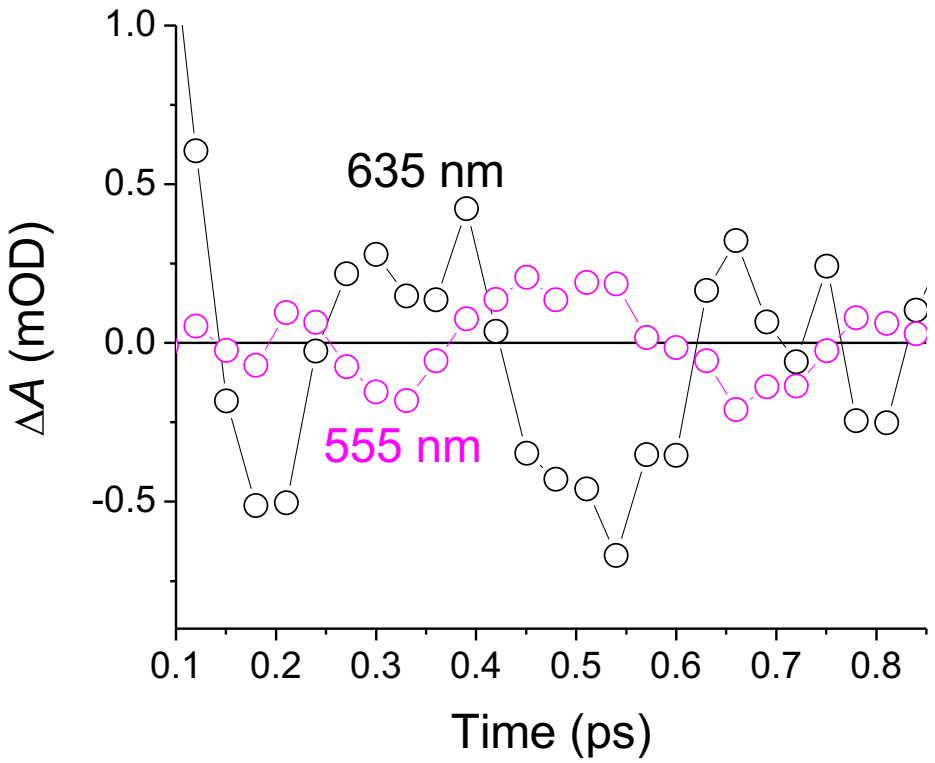

Fig. S24. The oscillations with a frequency of 101 cm^{-1} observed for Chrom7 following 925-nm excitation occur out-of-phase (a π-phase shift) in the blue and red wings (probe wavelengths: 555 and 635 nm) of the visible ESA band, providing evidence that the oscillations are due to the vibrational coherence in the excited S_1 state, the absorption from which is responsible for this ΔA band.

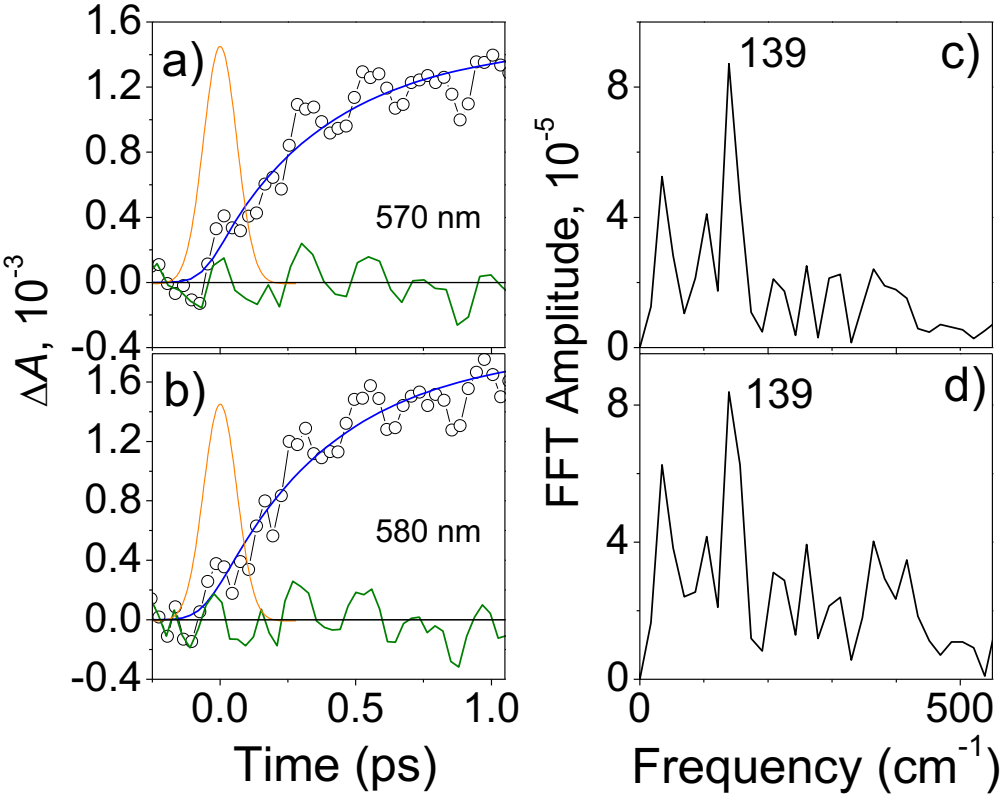

Fig. S25. The short-time ΔA kinetic traces (symbols), multiexponential fits (blue) with CCF deconvolution (a 145-fs fwhm, orange), and fit residuals (green) at 570- and 580-nm representative probe wavelengths following 500-nm excitation of Chrom7, a) and b). FFT analysis of the fit residuals in a) and b) is given in c) and d), respectively.

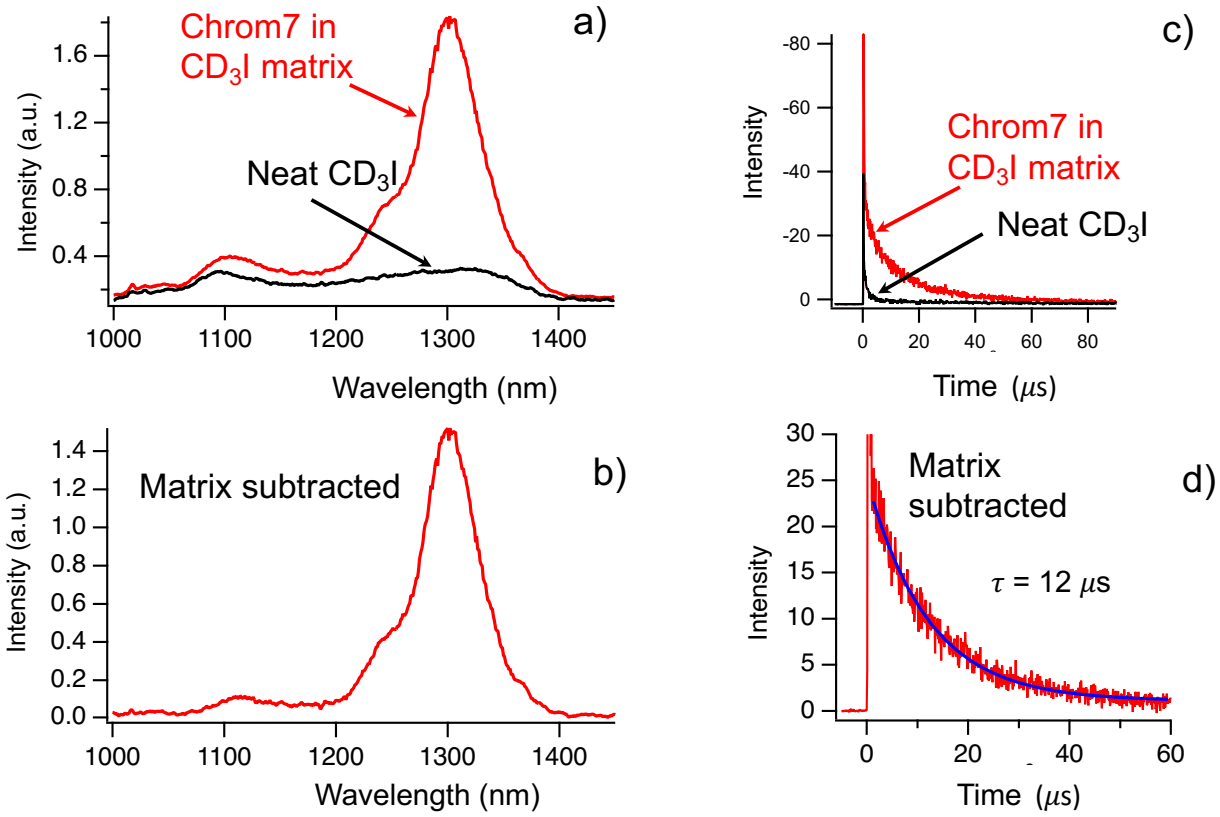

Fig. S26. The phosphorescence spectrum measured for Chrom7 kept in a 77 K in a CD_3I matrix, a). Liquid CD_3I was purged with N_2 prior to the experiment. The phosphorescence was recorded in the 4–19 μs time interval after pulsed (duration, 7 ns) laser excitation at 532 nm. The emission arising from excitation of the neat matrix under the same conditions is shown for comparison. The ~1260-nm shoulder is assigned to singlet oxygen emission,[9] whereas the broad feature from 1000 to 1190 nm is due to contributions from scattered fundamental (1064 nm) laser light and residual emission from the CD_3I matrix, which can be accurately subtracted. The phosphorescence spectrum of Chrom7 alone is presented in b), which is obtained by subtracting the two spectra shown in a). The emission decay for Chrom7 in a CD_3I matrix and the emission decay from the neat matrix measured under the same excitation conditions are shown in c). The detection wavelength was 1300 nm. The subtraction of the kinetic traces shown in c) yields the neat phosphorescence decay of Chrom7, d). The decay can be fitted to a single exponential with a 12 μs lifetime.

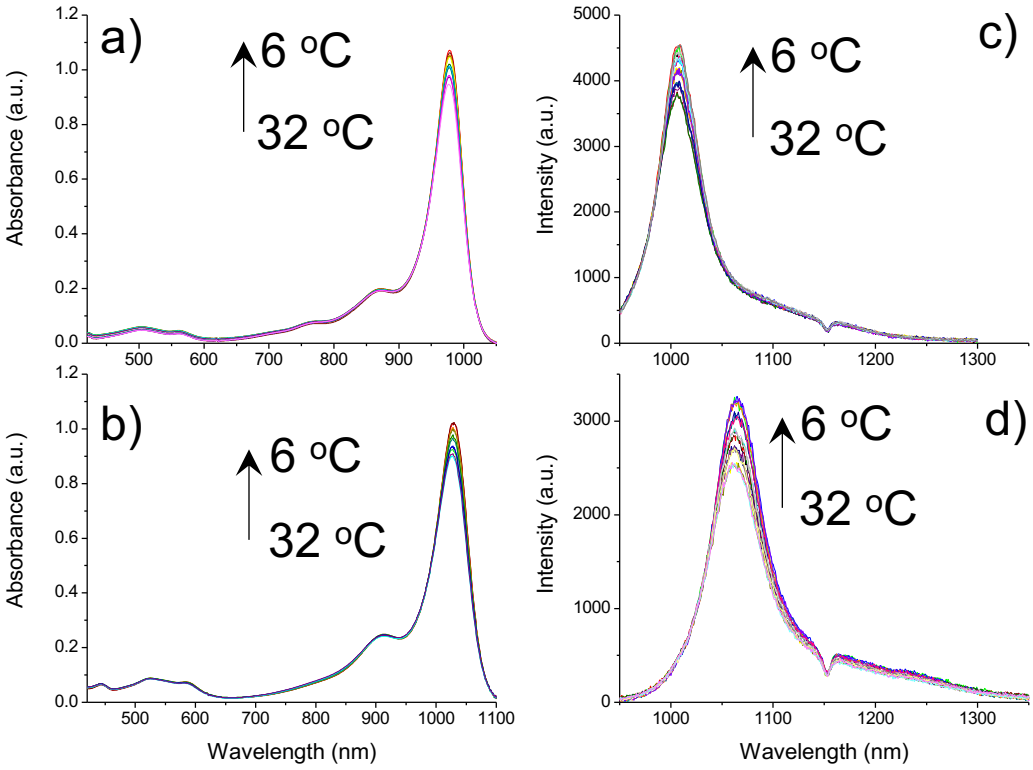

Fig. S27. Absorption spectra of Chrom7, a) and Flav7, b), and uncorrected fluorescence spectra of Chrom7, c) and Flav7, d) as a function of temperature between 6 and 32°C. The irradiation wavelength in the temperature-dependent fluorescence measurements was 900 nm. At this wavelength, the absorbance remains practically the same as temperature changes. The data were used to calculate the temperature dependence of the fluorescence quantum yield, see Experimental Section, main text, for more detail.

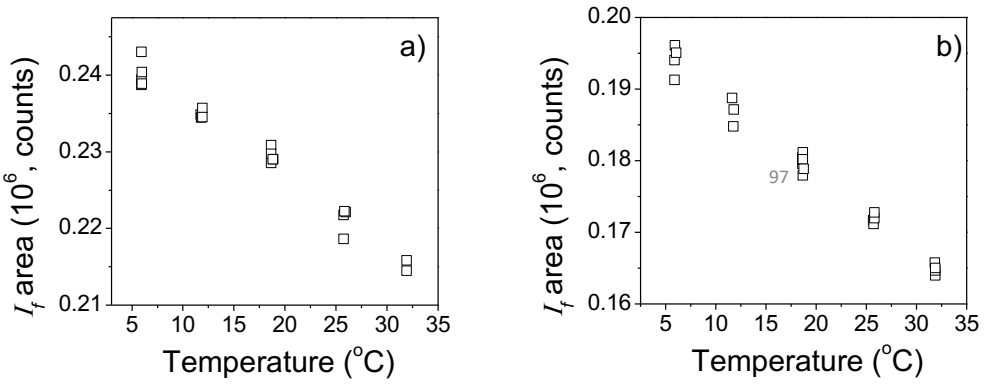

Fig. S28. The integrated areas under the fluorescence spectra (plotted on a y-axes) measured as a function of temperature are taken to represent the temperature dependence of the fluorescence quantum yield Φ_f. This assumption is valid because the change of the refractive index of $CHCl_3$ solvent within the investigated temperature range is very minor and the absorbance at the irradiation wavelength of 900 nm (Fig. S27) does not change appreciably with the temperature. The temperature variation of the measured areas is shown in a) for Chrom7 and in b) for Flav7.

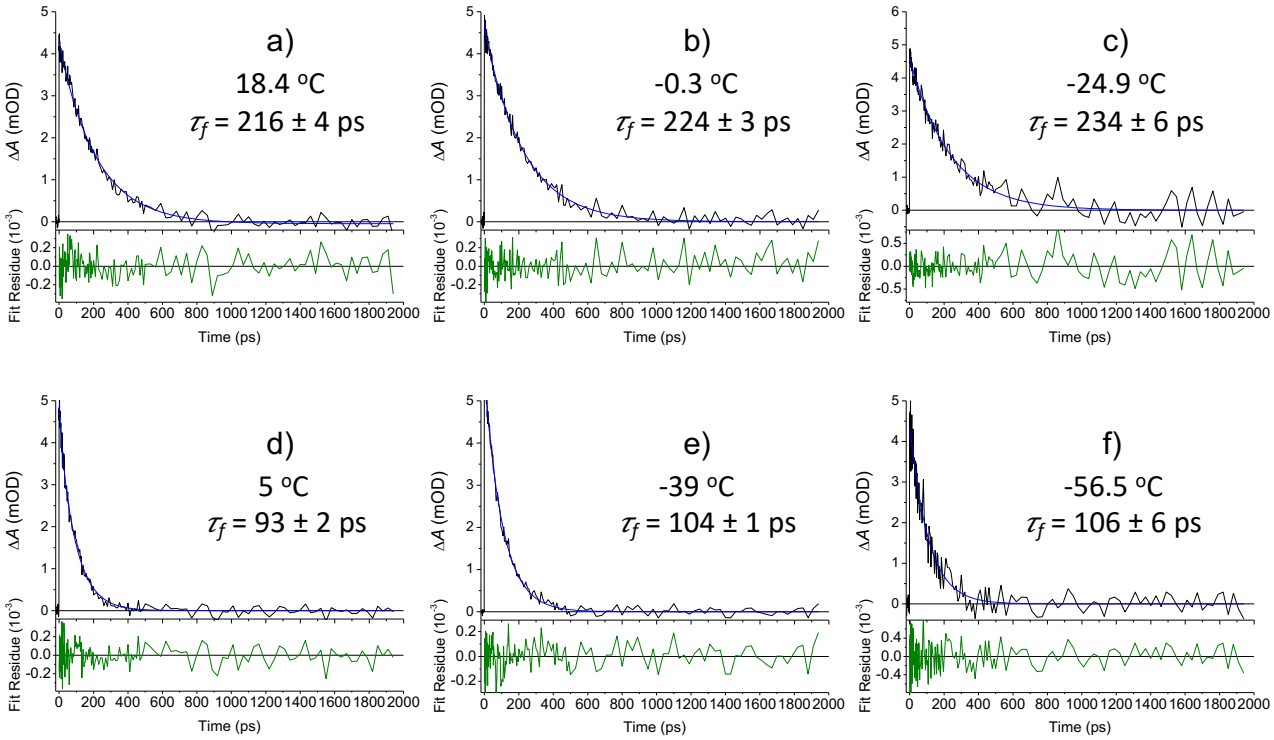

Fig. S29. Representative long-time ΔA kinetic traces for Chrom7, a-c) and Flav7, d-f) illustrating the influence of temperature on the S_1-state lifetime τ_f. The kinetic traces were fitted for delay times longer than 1 ps using a two-exponential decay model, where a minor component with several picosecond time constant was added to describe short-time dynamics not related to the population relaxation from the S_1 state. The best fit τ_f values are shown in the legends along with the experimental temperatures. Smaller panels show the fit residuals. The solvent is $CHCl_3$; the probe wavelengths used were 630 nm for Chrom7 (excitation, 990 nm) and 620 nm for Flav7 (excitation, 1042 nm).

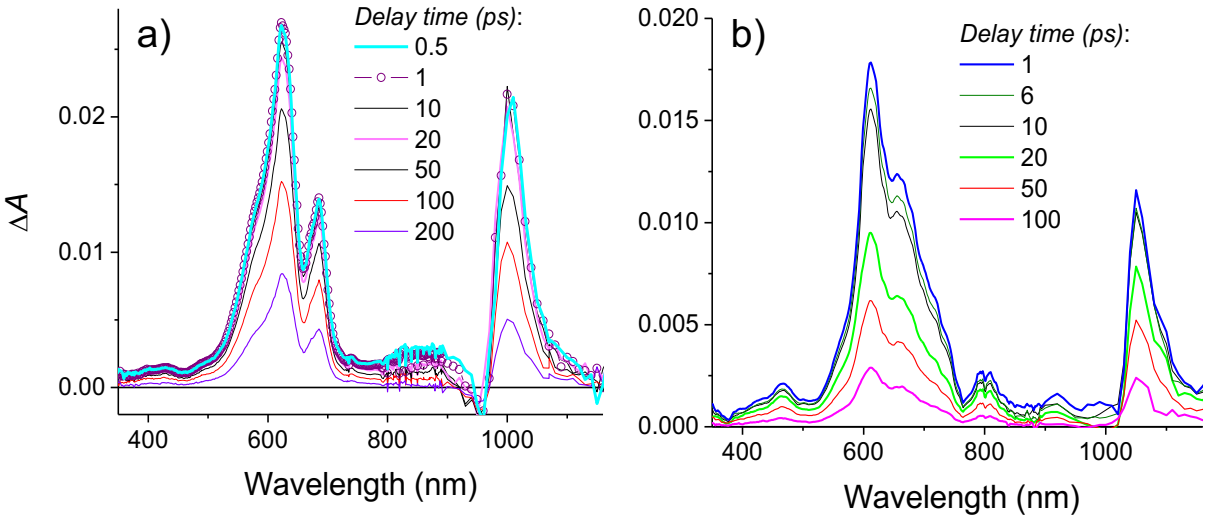

Fig. S30. Chrom7 excited at 990 nm, a), and Flav7 excited at 1042 nm, b). The shape of the S_1 excited-state absorption spectra, $\sigma_{ESA}(\lambda)$, shown for different delay times does not change with time. This is expected when ΔA signals are due to the following three contributions: ground-state absorption bleach, stimulated emission from S_1, and excited-state absorption from S_1, and in addition, when (i) S_1 is vibrationally equilibrated, (ii) vibrational relaxation in S_0 is much faster than the S_1 decay, and (iii) photochemical change is very minor or absent. To obtain the $\sigma_{ESA}(\lambda)$ spectral shapes, a sum of the $\sigma_A(\lambda)$ ground-state absorption and $\sigma_{SE}(\lambda)$ stimulated emission cross-section was fitted to the experimental ΔA spectra between 875-970 nm (Chrom7) and 960-1020 nm (Flav7). These spectral intervals were chosen because the aforementioned spectral curves closely match each other in these regions (Fig. 8 and the main text, see also Fig. S31). At delay times shorter than 500 fs, the S_1 state is not equilibrated, and this approach cannot be used.

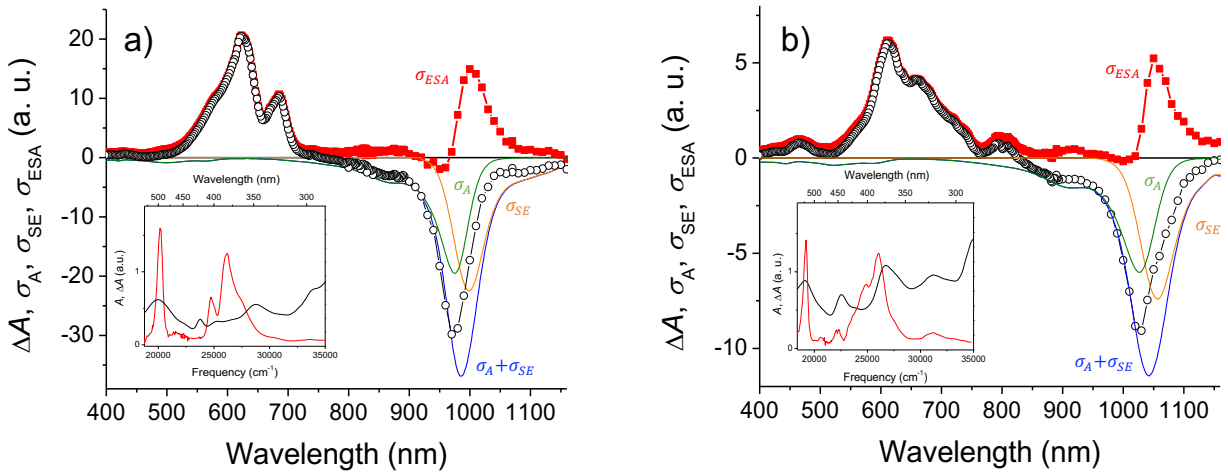

Fig. S31. Chrom7 excited at 990 nm in a), and Flav7 excited at 1042 nm in b). The ground-state absorption cross-section $\sigma_A(\lambda)$ and the S_1-state stimulated emission cross-section $\sigma_{SE}(\lambda)$ spectra are shown: $\sigma_A(\lambda)$ is determined from the molecular extinction spectrum and the maximum $\sigma_{SE}(\lambda)$ values are determined on the basis that S_0-S_1 and S_1-S_0 transition dipole moments are the same, see the main text. The $\sigma_A(\lambda) + \sigma_{SE}(\lambda)$ spectrum is then scaled to the experimental 50-ps ΔA spectrum (symbols) in the 875-970 nm (Chrom7) and 960-1020 nm (Flav7) range, where these spectra closely match each other and spectral amplitude changes rapidly so that the spectra can be scaled with the minimal uncertainty. The difference between the 50-ps ΔA and scaled $\sigma_A(\lambda) + \sigma_{SE}(\lambda)$ spectra yields the S_1 excited-state absorption $\sigma_{ESA}(\lambda)$ spectrum. The amplitude in the $\sigma_{ESA}(\lambda)$ spectrum reaches 9.2 10^{-16} cm^2 at 612 nm for Flav7 and 9.8 10^{-16} cm^2 at 622 nm for Chrom7. The above scaling procedure used to separate the $\sigma_{ESA}(\lambda)$ spectrum works for delays longer than 500 fs, but not at shorter times at which the S_1 states are not yet equilibrated. The insets compare the 50-ps ΔA spectra shifted along the energy scale by the S_0-S_1 electronic transition energy (10140 cm^{-1} in Chrom7 and 9700 cm^{-1} in Flav7) with the S_0-S_n linear absorption spectra. There is a general agreement between the energy positions of S_n, which is expected if ESA from S_1 occurs into the same terminal S_n states as the absorption from S_0. For Flav7, the S_n positions are 19120 cm^{-1} (522 nm), 22572 cm^{-1} (443 nm), and 23810 cm^{-1} (420 nm) based on the absorption maxima, and 19219 cm^{-1} (520 nm), 22278 cm^{-1} (448 nm) and 26036 cm^{-1} (384 nm) based on the maxima in the 50-ps ΔA spectrum shifted by 9700 cm^{-1}. For Chrom7, the S_n positions are 19878 cm^{-1} (503 nm), 23749 cm^{-1} (421 nm), and 25316 cm^{-1} (395 nm) based on the absorption maxima, and 20142 cm^{-1} (496 nm), 24732 cm^{-1} (404 nm) and 26200 cm^{-1} (382 nm) based on the 50-ps ΔA spectrum shifted by 10140 cm^{-1}. We assumed that the absorption maximum at about ~1 μm corresponds to the terminal excited S_2 state in both dyes. The energy positions of S_n agree within 266 and 100 cm^{-1} for S_2 of Chrom7 and Flav7, respectively, and within 294–984 cm^{-1} for $S_{4,5}$ in both dyes. ESA from S_1 into S_3 is weak and structureless (see the ~700-900 nm range in the $\sigma_{ESA}(\lambda)$ spectra), and therefore, the exact position of S_3 is uncertain.

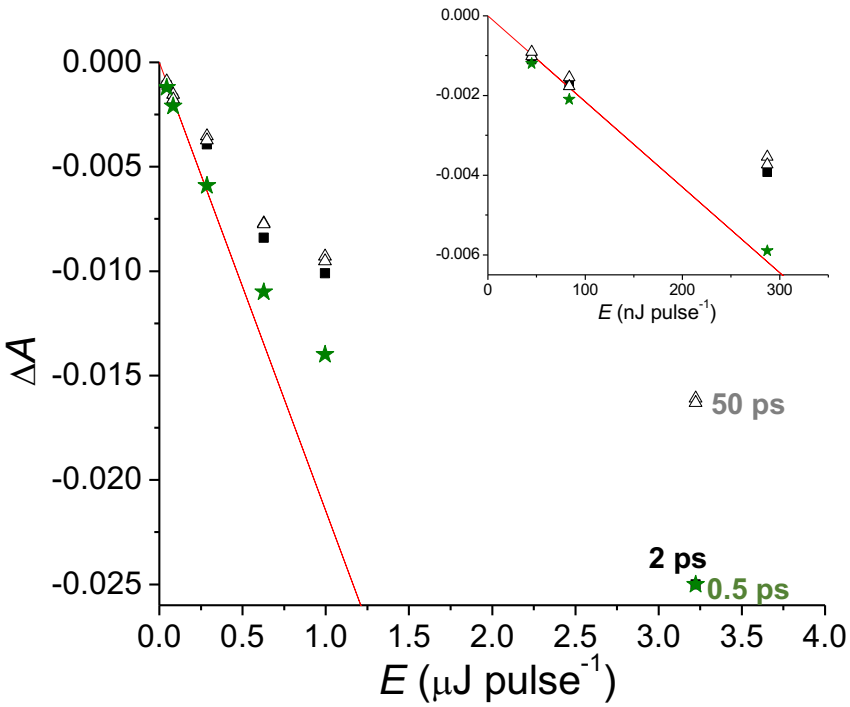

Fig. S32. The excitation energy dependence (symbols) of transient absorption measured at a 950-nm probe wavelength for Chrom7 in CH_2Cl_2 upon 990-nm excitation at several delay times between excitation and probe pulses: 0.5 ps (stars), 2 ps (solid squares), and 50 ps (open triangles). The excitation energy was varied by using calibrated neutral density filters. The linear fit through the 2-ps data set at low excitation intensity is shown. The saturation of the optical transition at high excitation fluences is evident. The inset shows the linear part of the excitation energy dependence; for single-photon excitation the energies of near-IR pulses utilized in the femtosecond transient absorption experiments on Chrom7 should not exceed 110 nJ pulse^{-1}.

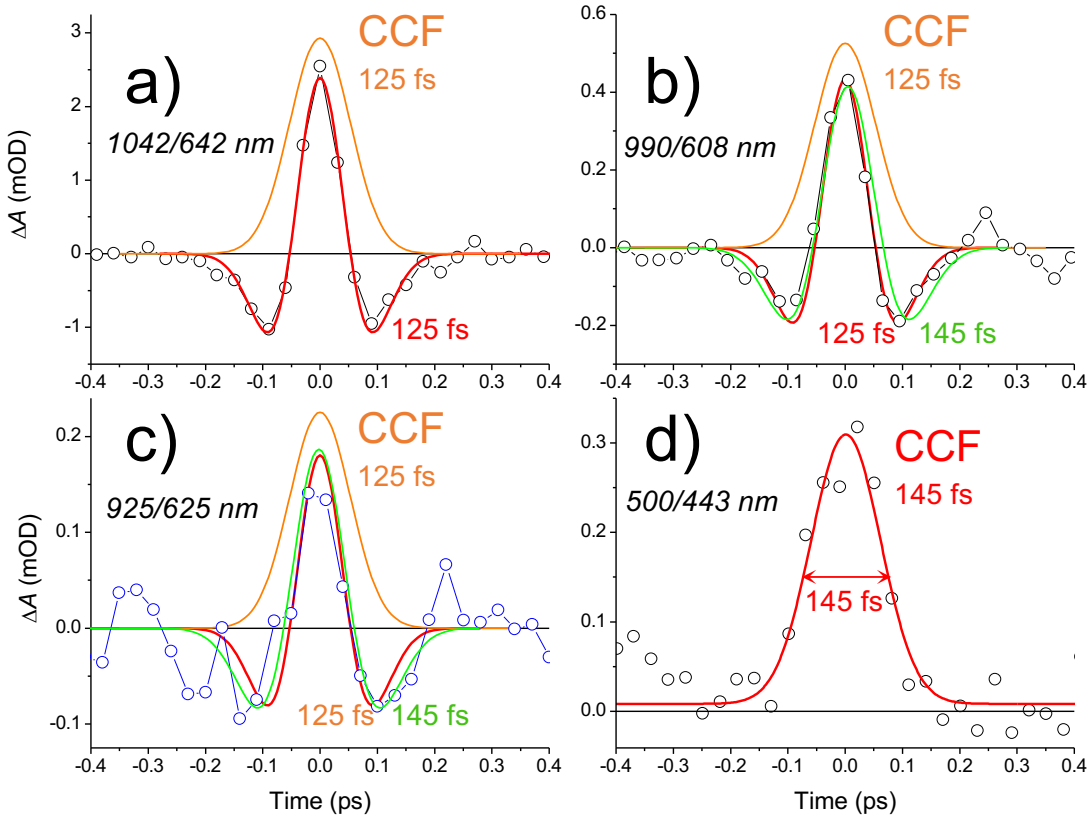

Fig. S33. Representative transient absorption signals (symbols) measured for neat CH_2Cl_2 at pump/probe wavelengths of 1042 nm/642 nm in a), 990 nm/608 nm in b), 925 nm/625 nm in c), and 500 nm/433 nm in d). These measurements were performed immediately after the sample measurement and at the same excitation conditions, apart from a), where excitation was about 700 nJ pulse^{-1}, i.e., ~10 times more intense than the one used for Flav7 and Chrom7 samples, e.g., b) and c). The ΔA signals in a-c) are the cross-phase modulation signals due to electronic instantaneous response of the solvent. The lines are the best fits to the data using the second time-derivative of a Gaussian-shaped function representing the pump/probe CCF,[5] where the CCF width is a fitting parameter. The best fits in a) and b) suggest a 125-fs width (fwhm), whereas a 145-fs fwhm shown in b) results in a poorer agreement. In c), the best-fit fwhm is 145 fs, with the 125-fs fwhm fit shown for comparison. The ΔA signal in d) shows strong anti-Stokes absorption at 433 nm at zero delay time,[7] which is due to the Raman-active C-H stretching mode of CH_2Cl_2 (3045 cm^{-1} [8]). The temporal shape of this signal, which is Gaussian in shape with a 145-fs fwhm, defines the CCF in the 500-nm excitation experiments reported in this work.

.

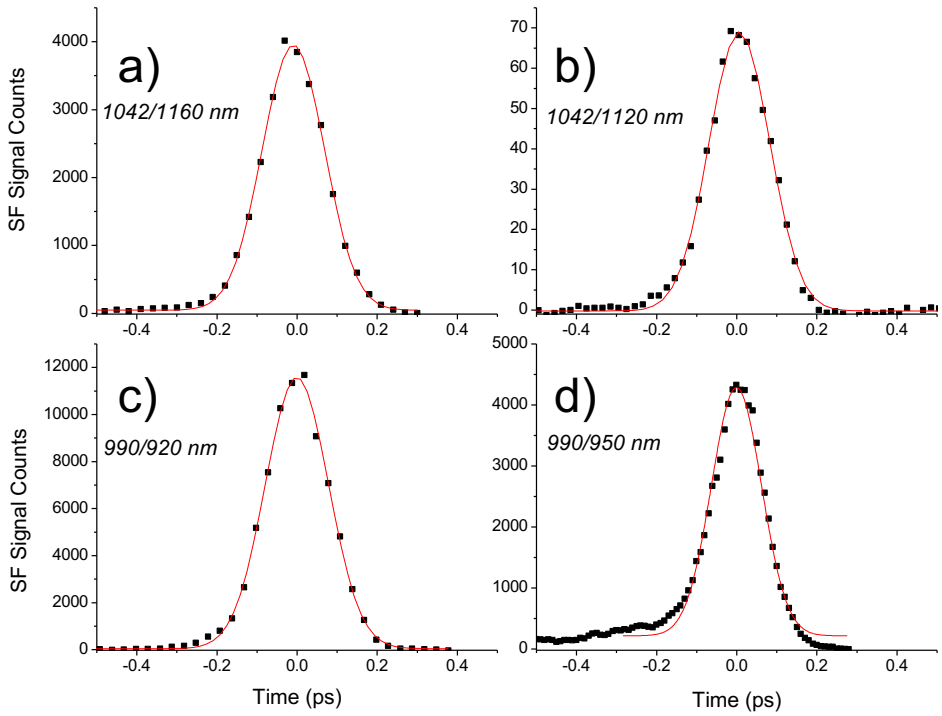

Fig. S34. Representative pump/probe 1042 nm/1160 nm in a), 1042 nm/1120 nm in b), 990 nm/920 nm in c), and 990 nm/950 nm in d) sum-frequency (SF) signals produced by non-linear mixing of the excitation and probe pulses at indicated wavelengths. The probe light source is an OPA, which output pulses were used in single-wavelength OPA-probe transient absorption experiments. The SF mixing intensity (symbols) was measured in a 0.1 mm thick type-1 BBO crystal at the same excitation conditions as the conditions used in transient absorption experiments. The temporal intensity profiles of the SF signals represent the excitation/probe CCF; the best fits of the SF intensities are found to exhibit a Gaussian shape with the width (fwhm) of 175 fs in a-b), 155 fs in c), and 145 fs in d). For evaluation of the shape and width of the CCF between the same excitation pulses and spectral components of the white-light continuum, see Fig. S33.

Table S1. Best-fit time constants characterizing the fastest component of hole dynamics for Chrom7 and Flav7 in CH_2Cl_2 following their excitation into the overlap of the S_0-S_1 absorption and S_1-S_0 fluorescence bands (0-0' vibronic shoulder) and into the 0-1' S_0-S_1 vibronic shoulder.

Excitation	λ_{exc} (nm)	Flav7	Chrom7	Probing Region
		τ_1 (fs) [a]		
0-0'	1042	350 [b]	–	GSB [b]
		58–125 [d]		ESA [c]
	990	–	230 [b]	GSB [b]
			58–125 [d]	ESA [c]
0–1'	925	57–125 [f]		ESA [e]
	925		53–125 [f]	ESA [e]

[a] The first component. The second component, τ_2, is about 1 ps for 0-0' and 0-1' excitations in both dyes, see ΔA kinetic traces in Fig. S5-S9 and Fig. S13-S15 and temporal spectral width analysis in Fig. S11 and Fig. S12.

[b] Probing the dynamics close to the bottom of the S_0 solute-solvent configurational potential following excitation at the low-energy side of the S_0–S_1 absorption spectrum, see Fig. 5, main text.

[c] Probing the dynamics on steeper parts of the S_0 solute-solvent configurational potential further away from the configurational well bottom.

[d] The range is defined by the time constants obtained by fitting the ΔA kinetic traces in Fig. S5-S8 and the temporal spectral widths in Fig. S11, and Fig. S12 (1042 and 990-nm excitation). We consider these time constants as the representative of the average time constant of 90±30 fs.

[e] Following 0-1' excitation, the dynamics within the S_1 ESA region is governed by both the S_1 and S_0 solute-solvent configurational potential, so the τ_1 time constant is representative of both ground-state hole and S_1 hole replica dynamics.

[f] The range is defined by the time constants obtained by fitting the ΔA kinetic traces in Fig. S15 and Fig. S16 and the temporal spectral widths in Fig. S11 and Fig. S12 (925-nm excitation).

Table S2. FFT frequencies of the modulations in the short-time ΔA kinetic traces measured for Chrom7 and Flav7 in CH_2Cl_2 following excitation of the solutions at different wavelengths.

	Excitation wavelength (nm)					
	Chrom7			Flav7		
	990	925	500	1042	925	500
Oscillation frequency (cm^{-1})	52 [a] 139 [b] 278 [c]	52 [d] 104 [e] 208 [e]	87 [f] 139 [g]	121 [i] 208 [j]	225 [k]	-

[a] Observed in 520-540 and 585-705 nm ranges, and at 570 nm
[b] Observed in the 545-605 nm range.
[c] Observed in the 520-540 range, and at 570 nm.
[d] Observed in the 580-600 range, and at 630 nm.
[e] Observed in the 550-650 range.
[f] Observed in the 410-460 range.
[g] Observed in the 470-610 range.
[i] Observed at 440, 585, and 785 nm.
[j] Observed in the 490-590 range.
[k] Observed in the 600-730 range.

Table S3. A summary of photophysical rate constants and quantum yields related to relaxation of the S_1 state in Chrom7 and Flav7.

	Product formation quantum yield [a]	k_{ph} (s^{-1}) [b]	τ_f (ps) [c]	k_{ic} (s^{-1}) [d]	$k_{ph}\tau_f$ [e]	ϕ [f]
Chrom7	$1.8 \cdot 10^{-3}$	$5.72 \cdot 10^{8}$	210	$4.03 \cdot 10^{9}$	0.12	0.014
Flav7	$6.4 \cdot 10^{-3}$	$3.88 \cdot 10^{9}$	77	$8.89 \cdot 10^{9}$	0.30	0.02

[a] Photoisomer product quantum yield. Estimated for CH_2Cl_2 solutions in the Section 'Ultrafast transient absorption: excitation into the low-energy part of the absorption spectrum', main text.

[b] Evaluated from the temperature dependence of the S_1-state lifetime, the Section 'Temperature dependence of the S_1 state lifetime', main text. Solvent: $CHCl_3$.

[c] As in footnote *b*, $CHCl_3$ solutions, 22 °C.

[d] As in footnote *b*, $CHCl_3$ solutions, 22 °C.

[e] The column entries are equal to the S_1 photoisomerization quantum yield, calculated using the k_{ph} and τ_f values, which were taken from the corresponding columns in this Table.

[f] The branching ratio ϕ evaluated as the ratio of the photoisomer formation quantum yield to the photoisomerization quantum yield in the S_1 state, $k_{ph}\tau_f$. This ratio in Chrom7 and Flav7 can be compared to penta- and heptamethine cyanines like DODCI and HITCI, where the excited S_1-state photoisomerization yield, $k_{ph}\tau_f$, is about 80%, the isomer product yield is about 8%, and consequently ϕ is about 0.1, see the Section 'Temperature dependence of the S_1 state lifetime', main text.

References

1 V. A. Gilbert and J. Baggott, Essentials of Molecular Photochemistry. Blackwell Scientific, Oxford, 1991, pp. 1–538.

2 G. Angulo, G. Grampp and A. Rosspeintner, Recalling the Appropriate Representation of Electronic Spectra, *Spectrochim. Acta. A*, 2006, **65**, 727–731.

3 S. K. Pal, A. S. Mereshchenko, E. V. Butaeva, P. Z. El-Khoury and A. N. Tarnovsky, Global Sampling of the Photochemical Reaction paths of Bromoform by Ultrafast Deep-UV through Near-IR Transient Absorption and ab initio Multiconfigurational Calculations, *J. Chem. Phys.*, 2013, **138**, 124501.

4 F. T. Gemeda, V. Vorobyev and A. N. Tarnovsky, Ultrafast Solution-Phase Photophysical and Photochemical Dynamics of Hexaiodobismuthate(III), the Heart of Bismuth Halide Perovskite Solar Cells, *J. Phys. Chem. B.*, 2022, **126**, 1254–1267.

5 S. A. Kovalenko, A. L. Dobryakov, J. Ruthmann and N. P. Ernsting, Femtosecond Spectroscopy of Condensed Phases with Chirped Supercontinuum Probing, *Phys. Rev. A*, 1999, **59**, 2369–2384.

6 K. Ekvall, P. van der Meulen, C. Dhollande, L.-E. Berg, S. Pommeret, R. Naskreski and J.-C. Mialocq, Cross Phase Modulation Artifact in Liquid Phase Transient Absorption Spectroscopy, *J. Appl. Phys.*, 2000, **87**, 2340–2352.

7 S. A. Kovalenko, N. P. Ernsting and J. Ruthmann, Femtosecond Hole-Burning Spectroscopy of the Dye DCM in Solution: the Transition from the Locally Excited to a Charge-Transfer State, *Chem. Phys. Lett.,*1996, **258**, 445–454.

8 H. J. Marrinan and N. Sheppard, Relative intensities of the Raman Lines of Carbon Tetrachloride, Chloroform, and Methylene Chloride, *J. Opt. Soc. Am.*, 1954, **44**, 815–819.

9 C. Schweitzer and R. Schmidt, Physical Mechanisms of Generation and Deactivation of Singlet Oxygen, *Chem. Rev.*, 2003, **103**, 1685–1757.

10 T. Bultmann and N. P. Ernsting, Competition between Geminate Recombination and Solvation of Polar Radicals following Ultrafast Photodissociation of Bis(p-aminophenyl) Disulfide, *J. Phys. Chem.* 1996, **100**, 19417–19424.